

Excitonic Interactions and Stark Spectroscopy of Light Harvesting Systems

Oscar J. G. Somsen,^{†,‡} Vladimir Chernyak,[†] Raoul N. Frese,[‡] Rienk van Grondelle,[‡] and Shaul Mukamel^{*,†}

Department of Chemistry, University of Rochester, P.O. RC Box 270216 Rochester, New York 14627-0216, and Department of Physics and Astronomy, Free University, De Boelelaan 1081, 1081 HV Amsterdam, Netherlands

Received: February 12, 1998; In Final Form: June 2, 1998

A closed expression for the Stark signal of molecular aggregates, which does not suffer from singularities when the exciton states are nearly degenerate and avoids the calculation of two-exciton states, is derived from the third order response to the total (static + optical) field, treating intermolecular interactions within the local field approximation. Transitions between one-exciton states play an important role and generally reduce the magnitude of the signal with respect to monomer spectra. The experimental Stark spectrum from the B820 dimer subunit of LH1 is consistent with simulations for a dimer of parallel pigments. The spectra of LH1 and LH2 cannot be explained by excitonic interactions alone. This supports the idea that charge-transfer states may play an important role in the spectroscopy of photosynthetic pigment proteins.

1. Introduction

Excitons play a crucial role in primary photosynthesis. They are created when sunlight is absorbed in light-harvesting proteins and then transferred between pigments until they reach a reaction center protein where, finally, they induce the primary charge separation. The nature of the excited states, can be probed with Stark (electroabsorption) spectroscopy, a technique whereby an electric field is applied to the sample. The resulting absorption changes yield information on the electronic properties of the excited states.¹ In the study of photosynthesis, Stark spectra were initially measured for reaction centers,^{2–4} and later also for light harvesting proteins.^{5,7,8}

To analyze such Stark spectra, a formalism has been developed by Liptay,¹ based on second-order perturbation, in the applied static electric field, of transition frequencies and transition dipole moments of a multilevel molecule. Solvent dynamics were included through a semiclassical treatment of the reaction fields, but can be ignored for the low temperature glasses discussed in this paper. For molecules with continuous absorption bands, the difference Stark spectrum, which is obtained by introducing a phenomenological line width, is a linear combination of the zeroth, first, and second derivative of the absorption spectrum.

This approach results in a perturbed eigenstate expression (PEE), which is given in eq A4. When the transition frequencies are well separated compared with the line width, the second-derivative contribution is determined only by the differences in permanent dipole moment between the excited state and the ground state and the first-derivative contribution by the difference in static polarizability. In that case, the PEE expression assumes a simpler form (PEE2, eq A6) which is commonly used.^{4–8} Unfortunately, the calculation of the Stark signal of a molecular aggregate, using the PEE is problematic, because the one-exciton levels can be arbitrarily close. This violates the conditions for the PEE2 and leads to singularities. These only cancel out when the full (PEE) expression is used, which requires explicit calculation of all one- and two-exciton states as well as transition polarizabilities and hyperpolarizabilities. Even though the singularities eventually cancel, their appearance

greatly complicates both numerical calculations and their interpretation.

In this paper we derive a new Green function expression (GFE) for the Stark signal of molecular aggregates, starting with the third-order nonlinear response to the total (optical + static) field. The Stark spectrum is expressed as a sum type I and II contributions. The former have the shape of the first and second derivative of the line shape function, and are related to the PEE2. Type II contributions, however, depend on transitions within the one-exciton band, and interpolate between the zeroth, first- and second-derivative shapes. The GFE does not suffer from singularities whose cancellation is naturally built in from the outset. Moreover, within the local field approximation, only one-exciton states need to be calculated. The GFE is thus more suitable than the PEE for calculating the Stark spectra of molecular aggregates such as photosynthetic pigment protein complexes. Moreover, the present approach makes it possible to connect Stark spectroscopy to different models for dynamics and relaxation of the molecules and their environment¹³ developed for nonlinear response theory, and to relate it to other third-order measurements.

In section 2 the GFE for the Stark signal is derived and compared to that for the PEE. In section 3 the GFE is used to calculate the Stark spectra of symmetric dimer and ring aggregates. These illustrate the significance of type II contributions in the GFE, and set the stage for the applications made in the following two sections. In section 4 we apply this theory to B820 dimers and the full LH1 and LH2 antennae are considered in section 5. Comparison with experiment is made for all systems. Finally, we summarize our results in section 6.

2. Green Function Calculation of Stark Spectra of Molecular Aggregates

We consider an aggregate made out of N three-level molecules. In the n th molecule the respective energies of the three states are 0, $\hbar\Omega_n$, and $\hbar\Omega_n^{(2)}$. We consider only the $S_0 \rightarrow S_1$ and $S_1 \rightarrow S_2$ transitions, with parallel transition dipole moments $\vec{\mu}_n$ and $\kappa_n\vec{\mu}_n$, respectively. In addition, the third-order

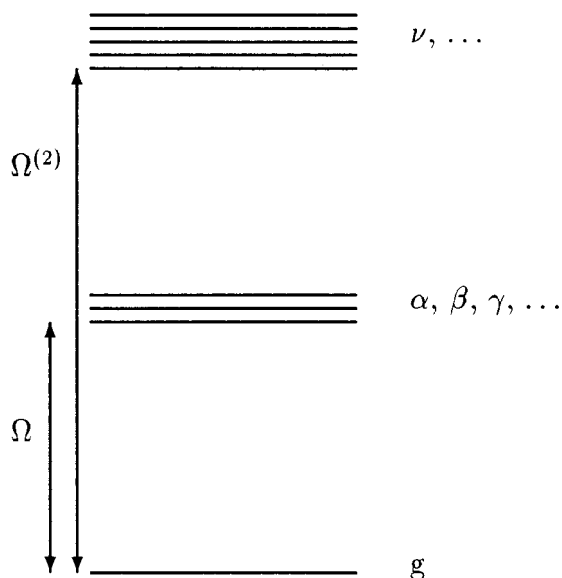


Figure 1. Schematic representation of the level scheme of an aggregate of N three-level molecules. The levels that are relevant for the third order response are a single ground state (g), a one-exciton band composed of N one-exciton levels (α, β, \dots), and a two-exciton band (ν, \dots), which consists of linear combinations of $N(N-1)$ two-exciton states with N biexciton states. The optical gaps Ω and $\Omega^{(2)}$ are defined as the frequencies of the lowest energy levels in consecutive bands.

response also depends on $\Delta\bar{\mu}_n$, the difference between the permanent dipole moments of S_1 and S_0 . The electronic state of the aggregate can be represented by introducing exciton annihilation operators: $B_n = |0_n\rangle\langle 1_n| + \kappa_n|1_n\rangle\langle 2_n|$, and their Hermitian conjugates, (creation) operators B_n^\dagger . These satisfy the following commutation relations:

$$[B_m, B_n^\dagger] = \delta_{nm}(1 - (2 - \kappa_m^2)B_m^\dagger B_m) \quad (1)$$

(an additional $(B_n^\dagger)^2(B_n)^2$ term has been omitted from the right-hand side of eq 1 because it does not affect the third-order response). Using these operators, the Hamiltonian can be expressed as¹⁴

$$H = \sum_n [\hbar\Omega_n B_n^\dagger B_n + \frac{1}{2}g_n(B_n^\dagger)^2(B_n)^2] + \sum_{nm} J_{nm}(B_n^\dagger B_m + B_m^\dagger B_n) \quad (2)$$

where $g_n = 2\hbar(\kappa_n^{-2}\Omega_n^{(2)} - \Omega_n)$ denotes the nonlinearity of the n th molecule, and J_{nm} the electrostatic interaction between molecules n and m . The dipole operator is

$$\hat{\mu} = \sum_n \bar{\mu}_n(B_n^\dagger + B_n) + \Delta\bar{\mu}_n B_n^\dagger B_n \quad (3)$$

Because the intermolecular interaction J_{nm} in eq 2 conserves the number of excitons, the eigenstates of the aggregate are grouped into independent bands, as illustrated in Figure 1. Relevant for the third-order response are the ground state g , the one-exciton states α, β, \dots , and the two-exciton states ν, \dots . The frequency of the lowest state in each band is denoted by the optical gaps Ω and $\Omega^{(2)}$. We assume that the one-exciton bandwidth is small compared with Ω , and that $\Omega^{(2)} \approx 2\Omega$, so that in off-resonant contributions, the one- and two-exciton frequencies can be replaced by Ω and 2Ω , respectively. Moreover $\hbar\Omega \gg k_B T$ so that only the ground state is occupied

at thermal equilibrium. These conditions typically hold for molecular aggregates.

We proceed to calculate the differential Stark (electroabsorption) signal $S_E(\omega)$ using the third order response function of the aggregate. The total electric field is composed of an optical (E_0) and a static field (E_s).

$$E(t) = E_0 e^{-i\omega t} + E_0^* e^{i\omega t} + E_s \quad (4)$$

The third-order response to this field contains frequencies between -3ω and 3ω .¹⁵ Relevant for absorption changes, such as the Stark signal, is the response at frequencies $\pm\omega$, which can be realized by either zero or two interactions with the static field. The former describes nonlinear absorption, and the latter the Stark signal $S_E(\omega)$ as follows:

$$S_E(\omega) = 3\text{Im}[\chi^{(3)}(-\omega; 0, 0, \omega)] E_0^* E_s E_0 \quad (5)$$

The two zero frequencies in $\chi^{(3)}$ refer to the interactions with the static field, and the frequency ω to the interaction with the optical field. The absorption change $S_E(\omega)$ is obtained by mixing the nonlinear response with the incoming field and is thus a product of a fourth-rank tensor (the third-order susceptibility $\chi^{(3)}$) and four fields. The signal $\langle S_E(\omega) \rangle$ for isotropic samples can be obtained by averaging over all molecular conformations. This procedure is discussed in Appendix B.

To evaluate eq 5 for the molecular aggregate defined by eq 1–3, we set up equations of motion for B_n and B_n^\dagger in the Heisenberg picture and solve these with a Green function approach.^{14–16} Expressions which give $\chi^{(3)}$ in terms of the one-exciton Green function and exciton–exciton scattering matrix were first derived for an assembly of two-level molecules.¹⁶ The GFE was later extended to an assembly of three-level molecules¹⁴ and to a two-band model in semiconductor systems.^{17,18} Exciton-phonon coupling has also been incorporated.^{19,20}

Since we are interested in the signal in the vicinity of $\omega = \Omega$, i.e., far from two-exciton resonances, the local field (or time-dependent Hartree–Fock) approximation can safely be applied.¹⁹ $\chi^{(3)}$ is given by eight contributions (eqs E.1 in ref 21). Within the rotating wave approximation (RWA), one would only retain terms that are resonant, i.e., express $S_E(\omega)$ to zeroth order in the ratio (Γ/Ω) of the dephasing rate (Γ) and the optical gap (Ω). This approach would yield only the first term of eq 6, which is not satisfactory for this type of signal, because it would vanish in the absence of permanent difference dipole moments (compare eq 9). To cover this case, we use a modified RWA by retaining also terms of first order in Γ/Ω , provided they do not include permanent dipoles. While these terms scale with Γ/Ω , which may be small, they are significant because they depend on transition dipole moments (compare eq 9) which are often larger than permanent dipole moments. The leading terms are $R_4^{(3)}$ (eq E.1d) and $R_6^{(3)}$ (eq E.1f). We thus obtain the Green function expression (GFE) of the Stark signal:

$$S_E(\omega) = \left(-\frac{1}{\hbar}\right)^3 \text{Im} \left[\sum_{\gamma, \beta, \alpha} \mu_{\gamma\beta} D_{\gamma\beta}^{(1)} D_{\beta\alpha}^{(1)} \mu_{\alpha\gamma} J_{\gamma\beta}(\omega) I_{\beta\gamma}(\omega) I_{\alpha\gamma}(\omega) - \sum_{\beta, \alpha} \mu_{\beta\alpha} D_{\beta\alpha}^{(2)} \mu_{\alpha\gamma} J_{\beta\gamma}(\omega) I_{\alpha\gamma}(\omega) \frac{1}{\Omega} \right] E_0^* E E E_0 \quad (6)$$

Here

$$I_{\alpha\gamma}(\omega) = 1/(\omega - \Omega_\alpha + i\Gamma) \quad (7)$$

is a complex line shape function, with Ω_α the frequencies of the one-exciton states and Γ a dephasing rate introduced into the equations of motion for the B_n , to represent coupling to a heat bath.¹⁵ The transition dipoles $\mu_{g\alpha}$ and the $D_{\alpha\beta}^{(j)}$ are given in the exciton basis set $\phi_\alpha(n)$:

$$\begin{aligned}\mu_{g\alpha} &= \sum_n \bar{\mu}_n \phi_\alpha(n) \\ D_{\alpha\beta}^{(j)} &= \sum_{nm} \phi_\alpha^*(m) D_{nm}^{(j)} \phi_\beta(n)\end{aligned}\quad (8)$$

The $\bar{\mu}_n$ were defined in the beginning of this section while the operators $D^{(1)}$ and $D^{(2)}$ have the following matrix elements in the molecular (site) representation:

$$\begin{aligned}D_{nm}^{(1)} &\equiv \delta_{nm} \Delta \bar{\mu}_m \\ D_{nm}^{(2)} &\equiv \delta_{nm} (\kappa_m^2 - 2) \bar{\mu}_m^* \bar{\mu}_n\end{aligned}\quad (9)$$

The first term of the GFE (eq 6) occurs within the RWA. It is determined by $D^{(1)}$ which indeed scales with the difference permanent dipole moments. The second term occurs only when the modified RWA is used. This term is proportional to $D^{(2)}$ which is related, but not identical, to the static difference polarizability ($\Delta\alpha$) in the PEE. For a monomer $\Delta\alpha = 2D^{(2)}/\Omega$ (see eq A5).

Equation 6 can alternatively be derived from the standard sum-over-states (SOS) expression of $\chi^{(3)}$. This is demonstrated in Appendix C. Both formalisms can also be applied under less restrictive conditions, e.g., without invoking the RWA, or by including more states and transitions. However, the GFE is computationally attractive, because two-exciton states need not be calculated within the local field approximation and because the occurrence of large canceling contributions, that is typical for the SOS formalism, is eliminated.¹⁵ Moreover, unlike the GFE the full SOS expression of the Stark signal contains diverging terms that can only be avoided by introducing a model for ground state relaxation.

The GFE (eq 6) provides an alternative to the standard PEE (perturbed eigenstate expression)¹ for the Stark signal discussed in the Introduction. In Appendix A, the PEE is recast in a form similar to the GFE. Let us compare the two approaches. In Appendix D we demonstrate that, within the modified RWA for which the GFE is given, it coincides with the PEE (eq A4). In the absence of intermolecular interactions this is obvious since $D^{(1)}$ and $D^{(2)}$ are, in that case, diagonal with $D_{\alpha\alpha}^{(1)} = \Delta\mu_{\alpha g}$ and $D_{\alpha\alpha}^{(2)}/\Omega = \Delta\alpha_{\alpha g}/2$, as discussed below eq 9. The general proof is more involved, because arbitrarily close energy levels give rise to singularities in α_{ab} and β_{ab} (see eq A5), which do not occur in the GFE. This also demonstrates that the simplified PEE2 (eq A6) which has been used successfully for semi-empirical analysis of experimental Stark spectra of photosynthetic pigment protein aggregates⁴⁻⁸ cannot be used to calculate the Stark signal from properties of the individual chromophores. To see this, consider two one-exciton states with a frequency difference that approaches zero. In that case, $\Delta\alpha$ approaches infinity (see eq A5) and eq A6 yields a spectrum with a first-derivative shape and infinite magnitude. In contrast, eq 6 remains finite and has a second-derivative shape. These singularities complicate numerical calculations, e.g., in the presence of inhomogeneous broadening when arbitrarily close energy levels do indeed occur. But, it also affects interpretation of experimental spectra, since a second derivative shaped Stark

spectrum is not necessarily due to a permanent dipole moment, but may also be caused by a transition to a nearby one-exciton state.

A close comparison of the GFE and PEE shows that the most striking difference is that the PEE contains only terms with powers of the line shape function. These will be denoted type I contributions. The imaginary part of $I(\omega)$ yields a Lorentzian line shape, and a straightforward calculation shows that the imaginary parts of $I^2(\omega)$ and $I^3(\omega)$ are the first and second derivative of this line shape. This is the basis of the more familiar description of the Stark spectrum as a linear combination of the zeroth, first, and second derivative of the absorption spectrum.^{1,5-8}

The GFE, however, contains additional products of different lineshape functions, which may be shifted with respect to each other, e.g., due to the exciton splitting or energetic disorder, or may ever differ in width of shape. Such contributions will be denoted as type II. Their structure and significance can be understood by expressing them as a sum of type I contributions (see eq D1). For example, the type II term $I_{\beta g}(\omega)I_{\alpha g}(\omega) = (I_{\beta g}(\omega) - I_{\alpha g}(\omega))/(\Omega_\beta - \Omega_\alpha)$ is the sum of two Lorentzians with opposite sign but takes the shape of a first derivative when $|\Omega_\beta - \Omega_\alpha| < \Gamma$. Similarly, a product of three line shape functions can take the shape of the zeroth, first, or second derivative of a Lorentzian. Thus, the type II contributions interpolate in a natural way between the various limiting cases. This eliminates singularities and makes the GFE preferable to the PEE, both for numerical calculations and for interpretation. Moreover, evaluation of the PEE requires the summation over all one- and two-exciton states, whereas only one-exciton states are needed for the GFE.

Note that if all dipole moments are the same, i.e., for all n : $\Delta\bar{\mu}_n = \Delta\bar{\mu}$, $\bar{\mu}_n = \bar{\mu}$, $\kappa_n = \kappa$, a special relation exists between the signal $S_E(\omega)$ and the ordinary absorption line shape $S_A(\omega)$ which has the form:

$$S_A(\omega) = \left(-\frac{1}{\hbar}\right) \text{Im} \left[\sum_\alpha \mu_{g\alpha} \mu_{\alpha g} I_\alpha(\omega) \right] E_0^* E_0 \quad (10)$$

Since in this case $D^{(1)}$ and $D^{(2)}$ are proportional to unit operators we get

$$S_E(\omega) = \frac{(\Delta\bar{\mu} E_s)^2}{2} \frac{d^2 S_A(\omega)}{d\omega^2} + (\kappa^2 - 2) \frac{(\bar{\mu} E_s)^2}{\Omega} \frac{dS_A(\omega)}{d\omega} \quad (11)$$

The signal $S_E(\omega)$ thus becomes a linear combination of the second and first derivatives of the absorption spectrum with coefficients independent of the size of the aggregate. This is significant for aggregates with parallel dipoles, such as J-aggregates. The deviation of the signal $S_E(\omega)$ from eq 11 provides a measure for the degree of inhomogeneity in dipole orientations.

3. Application to Dimers and Circular Aggregates

For symmetric aggregates, where only a few excitonic transitions are allowed, the GFE can be simplified. We shall demonstrate this for various dimeric and circular aggregates. The results will be used in the next sections to analyze experimental spectra of various light-harvesting complexes from purple bacteria.

We first consider the Stark spectrum of a monomeric pigment. With $\mu_1 = \mu$, $\Delta\mu_1 = \Delta\mu$, and $\kappa_1 = \kappa$, eq 6 reduces to

$$S_{E,\text{monomer}}(\omega) = \left(-\frac{1}{\hbar}\right)^3 \text{Im} \left[\mu \Delta \mu \Delta \mu \mu I_{1g}^3(\omega) - (\kappa^2 - 2) \mu \mu \mu \mu I_{1g}^2(\omega) \frac{1}{\Omega} \right] E_0^* E_s E_s E_0 \quad (12)$$

This expression contains only type I contributions (products of identical line shape functions), with the shape of the first and second derivative of the absorption spectrum, and in fact, coincides with the PEE2.

Let us first compare this to a dimer of parallel identical pigments. With $\mu_1 = \mu_2 = \mu$ and $\Delta\mu_1 = \Delta\mu_2 = \Delta\mu$, and one-exciton wave functions $\phi_{\pm}(n) = (\pm 1)^n / \sqrt{2}$, one obtains $\mu_{g+} = \sqrt{2}\mu$ while $\mu_{g-} = 0$. Also $D_{++}^{(1)} = D_{--}^{(1)} = \Delta\mu$ while $D_{+-}^{(1)} = D_{-+}^{(1)} = 0$, which means that $I_{+g}(\omega)$ is the only contributing line shape function. The second term in eq 6 can then be simplified by taking $I_{+g}(\omega)$ outside the summations. The result is independent of the molecular interaction and we have

$$S_{E,\text{dimer}}(\omega) = 2 \left(-\frac{1}{\hbar}\right)^3 \text{Im} \left[\mu \Delta \mu \Delta \mu \mu I_{+g}^3(\omega) - (\kappa^2 - 2) \mu \mu \mu \mu I_{+g}^2(\omega) \frac{1}{\Omega} \right] E_0^* E_s E_s E_0 \quad (13)$$

Remarkably, this expression is identical to that of the monomeric pigments, except for a shift from the monomer frequency to $I_{+g}(\omega)$. Since the linear absorption spectrum is shifted by the same amount, the excitonic interaction has no effect on the Stark spectrum for this geometry.

A very different behavior is found for an antiparallel dimer. With $\Delta\mu_1 = -\Delta\mu_2 = \Delta\mu$, we now obtain $D_{++}^{(1)} = D_{--}^{(1)} = 0$ while $D_{+-}^{(1)} = D_{-+}^{(1)} = \Delta\mu$, so that

$$S_{E,\text{dimer}}(\omega) = 2 \left(-\frac{1}{\hbar}\right)^3 \text{Im} \left[\mu \Delta \mu \Delta \mu \mu I_{+g}^2(\omega) I_{-g}(\omega) - (\kappa^2 - 2) \mu \mu \mu \mu I_{+g}^2(\omega) \frac{1}{\Omega} \right] E_0^* E_s E_s E_0 \quad (14)$$

The difference with the parallel dimer is that the expression now contains a type II contribution, i.e., a product of different line shape functions: $I_{+g}^2(\omega) I_{-g}(\omega)$. The origin of this difference is that the permanent dipole moment of the “+” state vanishes for an antiparallel dimer and is replaced by a transition from the “+” to the “-” state. As a result, the line shape functions of both excitonic states contribute to the Stark spectrum. The spectral shape of the type II contribution depends on the magnitude of the excitonic splitting (ω_{+-}) relative to the dephasing (Γ). When $\Gamma > \omega_{+-}$, we have $I_{+g}(\omega) \approx I_{-g}(\omega)$, and thus the term becomes a second derivative of the absorption, just as in the case of a parallel dimer. However, when $\Gamma \ll \omega_{+-}$, $I_{+g}^2(\omega) I_{-g}(\omega) \approx I_{+g}^2(\omega) \omega_{+-}$, which takes the shape of a first derivative. The physical explanation behind this is that, in that case, the “+” \rightarrow “-” transition contributes to the static polarizability of the former. The magnitude of the type II contribution is weaker than, or at most equal to, that of the corresponding type I contribution in the parallel dimer. More precisely, their ratio scales with Γ/ω_{+-} .

In summary, the Stark spectrum of a dimer differs from that of a monomer only when transitions are allowed within the one-exciton band. In that case a type II contribution interpolates between different type I shapes, while decreasing in magnitude, relative to the monomer case.

This behavior is typical and similar phenomena are found for ring-shaped aggregates. We first consider a ring with in-plane dipole moments, i.e., $\mu_n = |\mu|(\cos(n\xi)\hat{x} + \sin(n\xi)\hat{y})$ and

$\Delta\mu_n = |\Delta\mu|(\cos(n\xi)\hat{x} + \sin(n\xi)\hat{y})$, with $\xi = 2\pi/N$, and \hat{x} and \hat{y} two perpendicular unit vectors. The excitonic wave functions are $\phi_{\alpha}(n) = \epsilon^{i\xi\alpha n} / \sqrt{N}$, and only two transitions are allowed: $\mu_{g,\pm 1} = \frac{1}{2}\sqrt{N}|\mu|(\hat{x} \pm i\hat{y})$. Since these are degenerate, the second term of eq 6 is again not affected by the intermolecular interaction. Furthermore, $D_{\beta\alpha}^{(1)} = \delta_{\alpha,\beta+1}|\Delta\mu|(\hat{x} + i\hat{y}) + \delta_{\alpha,\beta-1}|\Delta\mu|(\hat{x} - i\hat{y})$. For a particular orientation of the aggregate, the expression for $S_E(\omega)$ is lengthy. However, for an isotropic sample, with magic angle ($\approx 54.7^\circ$) between the static and optical field, a number of terms vanish in the average signal. For this typical experimental situation, which is discussed in Appendix B, a more compact expression is obtained:

$$\langle S_{E,\text{ring}}(\omega) \rangle = N \left(-\frac{1}{\hbar}\right)^3 \frac{1}{9} \text{Im} \left[|\mu|^2 \left| \Delta\mu \right|^2 I_{1g}^2(\omega) \frac{I_{0g}(\omega) + I_{2g}(\omega)}{2} - (\kappa^2 - 2) \left| \mu \right|^4 I_{1g}^2(\omega) \frac{1}{\Omega} \right] |E_s|^2 |E_0|^2 \quad (15)$$

with $I_{\alpha g}(\omega)$ the complex line shape function of the pairwise degenerate excitonic states $\phi_{\pm\alpha}(n)$. This Stark spectrum differs from that of a monomer, in that it contains type II contributions from neighboring levels in the one-exciton band. However, the excitonic splitting between these levels is only a fraction of the intermolecular interaction strength, and is typically small compared to their line width, in which case the Stark spectrum reduces to that of the monomeric pigments.

For N even, a ring of antiparallel dimers can be modeled by simply reversing the orientation of every other pigment, i.e., by setting $\Delta\mu_n = (-1)^n |\Delta\mu|(\cos(n\xi)\hat{x} + \sin(n\xi)\hat{y})$. In that case $D_{\beta\alpha}^{(1)} = \delta_{\alpha,\beta+1/2N+1}|\Delta\mu|(\hat{x} + i\hat{y}) + \delta_{\alpha,\beta+1/2N-1}|\Delta\mu|(\hat{x} - i\hat{y})$, and thus (again for magic angle detection and isotropic samples)

$$\langle S_{E,\text{ring}}(\omega) \rangle = N \left(-\frac{1}{\hbar}\right)^3 \frac{1}{9} \text{Im} \left[|\mu|^2 \left| \Delta\mu \right|^2 I_{1g}^2(\omega) \frac{I_{1/2N g}(\omega) + I_{1/2N+2g}(\omega)}{2} - (\kappa^2 - 2) \left| \mu \right|^4 I_{1g}^2(\omega) \frac{1}{\Omega} \right] |E_s|^2 |E_0|^2 \quad (16)$$

In this case, the type II contribution combines line shape functions around frequencies from the top and bottom ends of the one-exciton band. As in the dimer case, the result can have either a second-derivative shape or a first-derivative shape with a weaker magnitude, depending on the width of the one-exciton band relative to Γ .

The differences between the parallel and antiparallel cases are important because Stark spectroscopy is one of the few techniques by which they can be distinguished. Note that the reversal of a pigment orientation has no effect on the absorption spectrum. The antiparallel structure has indeed been observed in the crystal structure of LH2.⁹ The Stark spectra of LH1 and B820 can be used to investigate the pigment orientation in these proteins.

4. Application to Subunits of the LH1 Antenna Complex

We shall now apply the general GFE (eq 6) and the compact analytical expressions for symmetric aggregates to calculate the Stark spectra of the light-harvesting systems from photosynthetic purple bacteria. Two types will be considered; The light-harvesting 1 (LH1) system, which forms a core complex with the reaction center, and LH2, which surrounds this core complex in variable numbers.

The main chromophore in these proteins is bacteriochlorophyll *a* (Bchl *a*). Its absorption of visible and near infrared light originates from an unsaturated π -electron system of approximately 1 nm radius, which runs across a porphyrin ring. The red-most (Q_y) transition absorbs at 780 nm, with a transition dipole moment along the long axis of the π -system. In LH1, this transition is significantly red shifted (to 880 nm), while LH2 shows two absorption bands (at 800 and 820–850 nm). Further transitions are the Q_x (600 nm) and Soret (B_y and B_x , 300–400 nm) transitions.

For the third-order optical response, only the three lowest electronic states are relevant, at least as long as transitions are allowed only between neighboring levels, (i.e., $S_0 \rightarrow S_1$, $S_1 \rightarrow S_2$, etc.). We shall thus model Bchl *a* as a three-level molecule with a ground state, Q_y and B_y (Soret) level. The aforementioned condition is not strictly fulfilled since the B_y transition is visible in the ground state absorption spectrum. But, since any contribution from this transition is off-resonant, it will be omitted. For the same reason, and because no transition is possible between the Q_y and Q_x levels, the Q_x and B_x levels are also omitted. The light-harvesting pigment–protein complex can thus be modeled by an aggregate of N three level molecules.

The structure of both LH1 and LH2 is a ring of subunits, each composed of a Bchl *a* dimer bound to two small (one helix) membrane bound polypeptides. The porphyrin rings are vertical, with the Q_y transition dipole moments forming a small angle ($<15^\circ$) with the membrane. The 800 nm transition of LH2 is caused by the presence of a third Bchl *a* pigment. In addition, the subunit may contain one or two carotene molecules.

High-resolution (0.25 nm) crystal structures of *Rhodospseudomonas (Rps.) acidophila* LH2 show a ring of nine dimer subunits,⁹ while *Rhodospirillum (Rsp.) molischianum* LH2 contains a ring of eight such subunits.¹⁰ Within each dimer, the pigments are almost antiparallel, while forming a small angle with the tangent of the ring. The interpigment distance within the dimer is almost identical to that between neighboring dimers (0.9 nm). Low-resolution (0.85 nm) structures of LH1¹¹ show a larger ring of 16 dimer subunits. Similarities of function and polypeptide sequence and structure modeling indicate that the pigment organization of LH1 must be very similar to that of LH2.

From LH1, a dimer (B820) subunit can be isolated by adding detergent.¹² The Q_y transition then shifts to 820 nm. Upon further addition of detergent, monomeric (B777) complexes are formed. The process is reversible and by diluting the sample it reassociates to a B873 complex which strongly resembles LH1, except for the carotene molecules (two per B820 subunit), which are lost during the dissociation. The Stark spectrum of the B820 subunit will also be discussed because it may form a bridge between those of LH1 and the monomeric pigments. So far it has not been possible to prepare similar subunits of LH2.

Using the PEE2 a semiempirical analysis has been carried out for the Stark spectra of photosynthetic proteins.^{4–8} In these studies, the B820 spectrum is dominated by a second derivative (of the absorption spectrum) shape, indicative of a difference dipole moment similar to that of monomeric Bchl *a*, while the spectra of LH1 and LH2 are much larger and dominated by a first derivative shape, indicative of a difference polarizability. In addition, a significant unexplained zeroth-derivative contribution is present especially in B820.

We shall further the analysis these experimental results by calculating the Stark spectra of the Bchl *a* aggregates. As we demonstrated, the PEE and PEE2 are not suitable for these calculations due to singularities, and we thus use the GFE (eq

6) and the compact analytical expressions derived for symmetric aggregates in the previous section. Rather than to try and adjust the numerous parameters to the Stark measurements, we shall start with parameters from related experiments, and then vary the parameters one by one, to investigate their effect on the spectra.

Two groups of parameters need to be considered, representing respectively the Bacteriochlorophyll *a* (Bchl *a*) chromophore itself, and their organization within the aggregate. The latter will be discussed separately for each light-harvesting protein, but the chromophore is described by a common set of parameters.

The $S_0 \rightarrow S_1$ Transition Dipole Moment. The value $\mu = 6.2$ D has been determined from absorption.^{22,23}

The Optical gap (Ω), Dephasing (Γ) and Energetic Disorder (σ , Defined Below). These spectral parameters change upon association with protein, and are adjusted to fit the absorption spectrum.

The Difference in Dipole Moment between the S_1 and S_0 States. This is especially significant for the Stark spectrum. A value of $\Delta\mu = 1.45 \pm 0.2$ D was obtained from Stark spectra of the monomer² with a Lorentz local-field correction factor. It forms a small angle (11°) with the transition dipole moment,³ but in our simulations we took them to be parallel.

The Relative Oscillator Strength of the $S_1 \rightarrow S_2$ Transition. This parameter is related to the difference polarizability in the PEE2, but it is an essential parameter for any non-linear response. In particular, a significant cancelation of the third-order response takes place for $\kappa = \sqrt{2}$. The value $\kappa = 1$ was estimated from excited state absorption.²⁴ This is, however, only a rough estimate. For example, a small positive difference polarizability $Tr[\Delta\alpha] = 36 \pm 6 \text{ \AA}^3$ was observed with solvent shift measurements,²⁵ which suggests that κ may actually be larger than $\sqrt{2}$. κ was therefore varied in our simulations.

In a number of calculations energetic (inhomogeneous broadening) and structural disorder are included. For the former, the optical gap of each pigment is changed by a random amount taken from a Gaussian distribution with variance σ , before calculating the Stark and absorption spectra. This procedure is repeated, and the spectra are averaged until convergence is reached. Structural disorder is incorporated by assuming that the dipole moment of each pigment is rotated by a random amount. This is achieved by setting up a local coordinate system with its z-axis along the dipole moment, and choosing a new dipole moment with polar coordinates (θ , ϕ) in that system. θ and ϕ are uniformly distributed random numbers in $[0, \theta_0]$ and $[0, 2\pi]$, respectively. Convergence was monitored by calculating not only the average signal for each data point, but also its standard deviation. Averaging was continued until all standard deviations are less than 3% of the maximum of the spectrum. This required between 250 ($N = 32$, $\sigma = \Gamma$) and 500 000 ($N = 2$, $\sigma = \Gamma/4$) iterations, and takes between one minute and several hours on a Silicon Graphics (Octane) workstation.

The surrounding medium is modeled by a Lorentz local-field correction factor. This gives the ratio of the internal field E_i felt by the molecule, to the externally applied field E_s :

$$E_i = \frac{\epsilon + 2}{3} E_s \quad (17)$$

and the dielectric constant ϵ was set to 2.

The experimental absorption and Stark spectra were reproduced from publications on monomeric Bchl *a*,²⁶ B873 (re-associated LH1) and B820 from *Rhodospirillum (Rsp.) rubrum*⁷

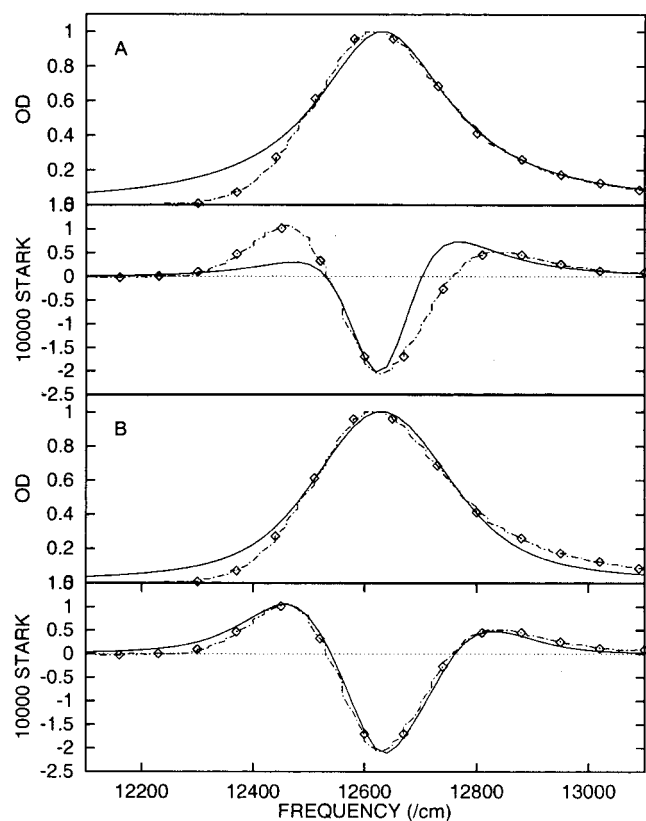


Figure 2. Simulated absorption and Stark ($=\Delta OD$ at $E_s = 10^5$ V/cm) spectra and experimental 77 K spectra (diamonds) for monomeric Bchl *a* in toluene/pyridine (100:1 v/v). (A) Calculation with $\Omega = 12630$ cm^{-1} , $\sigma = 0$, $\Gamma = 145$ cm^{-1} , and all other parameters taken from separate experiments (see text): $\mu = 6.2$ D, $\kappa = 1$, $\Delta\mu = 1.45$ D, and $\epsilon = 2.4$. (B) Best fit; $\sigma = \Gamma = 80$ cm^{-1} , $\kappa = 1.85$, and $\Delta\mu = 1.65$ D. Other parameters as in A. Experimental spectra reproduced from Lao et al.²⁶

and LH2 from *Rps. acidophila*.⁸ All experimental and simulated Stark spectra are shown with the corresponding normalized absorption spectrum. The Stark, i.e., the difference between the absorption with and without field, spectra are scaled to a normalized field of $E_s = 10^5$ V/cm.

A. The Bchl *a* Monomer. To test the parameter values given above, we first compare experimental and simulated spectra of the monomeric Bchl *a* pigment. Figure 2A displays the simulated absorption and Stark spectra with experiment. Only homogeneous broadening is included, and Ω and Γ are adjusted such that the simulated and experimental absorption spectra coincide at $OD = 0.5$. The magnitude of the experimental Stark spectrum and its second-derivative shape, caused by a $\Delta\mu$ -dependent term, are properly reproduced. Some deviations are obvious: the minor asymmetry caused by the κ -dependent term has the wrong sign in the simulated spectrum, and the experimental Stark spectrum appears to be broader than the simulated one. In Figure 2B parameters have been optimized to fit the spectra. Some energetic disorder has been introduced, which leads to a broadening of the Stark spectrum with respect to the absorption. Combined with a small increase of $\Delta\mu$ and κ , this leads to a satisfactory fit, although deviations in the wings are noticeable. The fit of the Stark spectrum is better than that of the absorption spectrum.

B. The B820 Dimer. Simulation of the Stark spectrum of the dimeric B820 subunit of LH1 requires in addition to the Bchl *a* parameter values given above, a model for the dimer geometry. Fluorescence polarization experiments¹² indicate that

the angle between the transition dipole moments of the two pigments is small ($<30^\circ$). We initially consider cases where the pigments are either parallel or antiparallel. The results can thus be compared to the analytical expressions in the previous section. For the intermolecular interaction we use $J_{nm} = 230$ cm^{-1} , as estimated from the same experiments.

In Figure 3, experimental absorption and Stark spectra for B820 are compared to simulations for the parallel and antiparallel dimer, for several inhomogeneity ratios σ/Γ between 0 and 4, and structural inhomogeneities θ_0 between 0 and 40° . For $\sigma/\Gamma = \theta_0 = 0$, Ω and Γ were adjusted with the same procedure as for the monomer. In all other spectra, the same value of Ω was used, while σ and Γ were varied to reproduce the fwhm of the experimental absorption spectrum.

The simulated Stark spectra for the parallel dimer resemble eq 13. For the homogeneous ($\sigma = 0$) case, they coincide, and in all cases, the spectra are dominated by a $\Delta\mu$ -dependent type I contribution, which has the form of a second derivative (of the absorption spectrum). As in the monomer spectra, a small asymmetry is present, due to the κ -dependent term. This term disappears for $\kappa = \sqrt{2}$ (compare Figure 4A). Except for a shift induced by excitonic splitting, the homogeneously broadened ($\sigma = 0$) spectrum is identical to that of the monomeric pigments with the same Γ (not shown). The other spectra in figure 3A are weaker, because the energetic disorder induces partially allowed “+” \rightarrow “-” transitions, and thus are type II contributions. These are smaller than the type I contribution to which they reduce when the material frequencies become equal.

Comparing the numerical and analytical results is less straightforward for the antiparallel dimer. The small magnitudes of the simulated spectra in Figure 3C confirm the analytical result of section 3: an antiparallel dimer has a smaller Stark spectrum than a parallel dimer, due to the presence of type II contributions for the former. But the shape of the simulated spectra (a negative and positive lobe at the lower and upper excitonic states respectively), does not seem to agree with the dominant first-derivative shape of such a type II contribution. This results from an interference of the $\Delta\mu$ - and κ -dependent terms which are, in this case, of the same magnitude

The effects of energetic and structural disorder on the Stark spectra are limited. The former leads to a red shift of both the absorption and Stark spectrum, but the absorption maximum remains coincident with the minimum of the Stark spectrum. In addition, energetic disorder causes broadening of the Stark spectrum and a decrease of the amplitude. The effects of structural disorder are marginal.

The experimental Stark spectrum is best reproduced by the simulated spectra in Figures 3A and B. This indicates that the B820 subunit may form a parallel dimer, in contrast to the antiparallel dimer that has been observed in the crystal structure of LH2.⁹ However, the fit is not quite satisfactory. The main difference is that the experimental Stark spectrum is broader than the simulated ones. This discrepancy is reduced but not quite eliminated, by the energetic and structural disorder (Figure 3A). In an earlier study, a better fit has been obtained with a linear combination of the zeroth and second derivative of the absorption spectrum.⁷ However, this required a substantial zeroth-derivative contribution, which cannot be justified by the present calculations. For example, eq 13 has no zeroth derivative contribution at all, and although the type II contribution in eq 14 has a zeroth-derivative component, this is considerably smaller than the other contributions. Moreover,

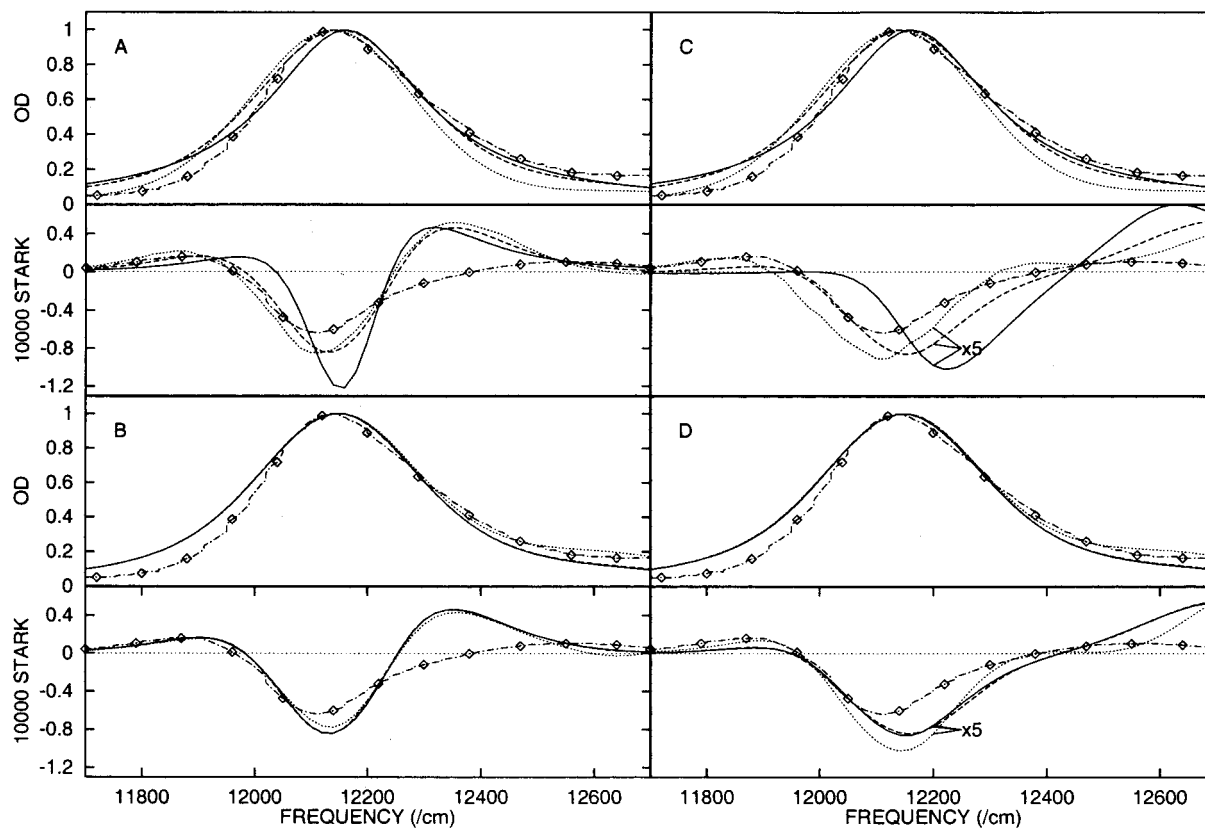


Figure 3. Simulated absorption and Stark ($=\Delta OD$ at $E_s = 10^5$ V/cm) spectra for a Bchl *a* dimer, and experimental 77 K spectra (diamonds) for the B820 dimer subunit from *Rsp. rubrum*. (A and B) Parallel dimer (see text) with (A) energetic disorder: $\sigma/\Gamma = 0$ (solid), 1 (dashed), and 4 (dotted). (B) Structural disorder: $\theta_0 = 0^\circ$ (solid), 10° (dashed), and 40° (dotted), for $\sigma = \Gamma = 120$ cm^{-1} . (C and D) Same calculations for the anti-parallel dimer (see text). Other parameters: $\Omega = 12390$ cm^{-1} , $\mu = 6.2$ D, $\kappa = 1$, $\Delta\mu = 1.45$ D. Intermolecular interaction: $J_{nm} = -230$ cm^{-1} . $\epsilon = 2.0$. As indicated, the simulated spectra in C and D are multiplied by 5. Experimental spectra reproduced from Beekman et al.⁷

it is compensated by a zeroth-derivative component of opposite sign at the high exciton component, which is also not observed in experiment. Somewhat smaller zeroth derivative components have also been derived from fits to Stark spectra from reaction centers⁴ and light-harvesting proteins,^{5,7,8} but no explanation has as yet been given.

Starting from Figure 3, we vary the parameters one by one to improve the fit to experiment. This is done for the parallel dimer only, since this seems the most likely structure. For computational efficiency, energetic and structural disorder are, for the time being, omitted, since these had little effect on the spectrum. In Figure 4A κ is varied between 0 and 2. The asymmetry is affected, which leads to a shift of the Stark spectrum relative to absorption. This can be used to fit different features of the experimental spectrum, but it does not increase the width of the spectrum, as required for a good fit. Similar effects are observed when $\Delta\mu$ or μ is varied (not shown).

We also tried to improve the fit by relaxing the symmetry of the aggregate. In Figure 4B, the angle between the pigments is increased up to 40° (the actual angle is estimated to be 24° ¹²). This leads to minor changes in the absorption and Stark spectrum near the upper exciton component, but its effect in the main band is limited to a small decrease of the magnitude of the Stark spectrum. Finally, we studied the effects of reducing the magnitude of the intermolecular interaction down to 60 cm^{-1} , and of lifting the degeneracy, by increasing the difference between the optical gaps of the two pigments up to 400 cm^{-1} (while keeping the excitonic splitting at 460 cm^{-1}). Both parameters had a negligible effect on the Stark spectrum (not shown). Especially the last result is somewhat remarkable

because the dimer, in that case, has two allowed transitions. In any case, the results indicate that the fit to experiment is not improved by relaxing the symmetry of the aggregate.

The parameter changes discussed above, which all lead to minor improvements of the fit were combined to produce our best fit that is shown in Figure 5. The main optimizations were A minor change of $\Delta\mu$ to exactly reproduce the magnitude of the spectrum and the reintroduction of energetic disorder to produce a satisfactory fit of the red flank of the Stark spectrum. The shallow blue feature, however, could not be fitted without ruining the overall fit (compare Figure 4A). Note that the resulting parameter set is not unique. For example, the effects of decreasing $\Delta\mu$ and $\kappa^2 - 2$ could also have been obtained by decreasing ϵ , and the structural disorder cannot be estimated from the fit at all, because its effect on the Stark spectrum (compare Figure 3B) is small.

In conclusion, the magnitude and approximate shape of the B820 Stark spectrum can be reproduced by a relatively simple model of a parallel dimer, with parameters derived from separate experiments. However, its shallow blue flank not explained by excitonic interactions alone. If it is not an experimental artifact, e.g., due to overlap with the 777 nm band of monomeric Bchl *a*, it requires either a new mechanism that adds a zeroth-derivative component to the Stark spectrum, or a more detailed model for line broadening, e.g., by adding vibrational transitions.

5. Application to the LH1 and LH2 Antenna Complexes

A. The LH1 Complex. We have applied our analysis strategy to investigate the experimental Stark spectrum of B873

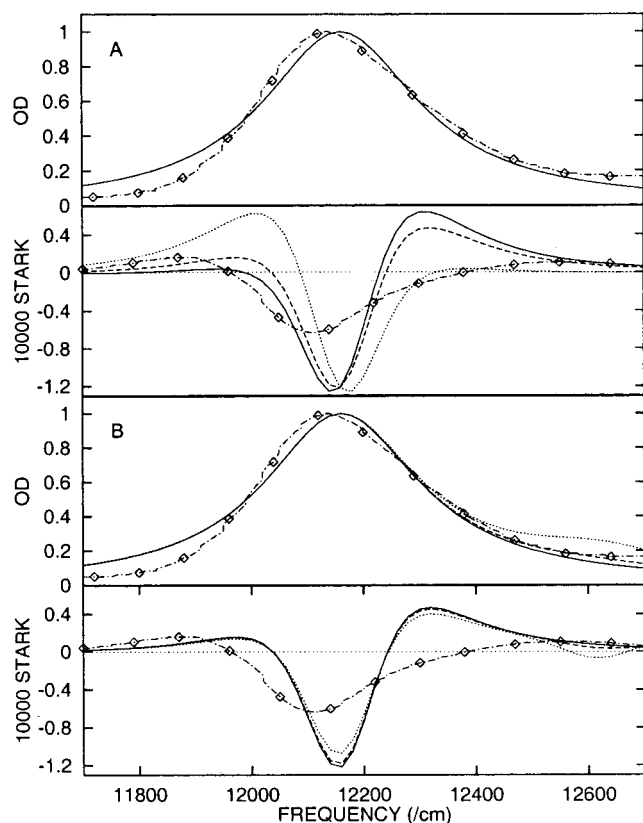


Figure 4. Simulated absorption and Stark ($=\Delta OD$ at $E_s = 10^5$ V/cm) spectra for a parallel Bchl *a* dimer, and experimental 77 K spectra (diamonds) for the B820 dimer subunit from *Rsp. rubrum*. (A) $\kappa = 0$ (solid), 1 (dashed), and 2 (dotted). In (B) the angle between the pigments is increased from 0° (solid), to 10° (dashed), and 40° (dotted). Other parameters: $\sigma = 0$, $\Gamma = 170$ cm^{-1} , and additionally as in Figure 3. Experimental spectra reproduced from Beekman et al.⁷

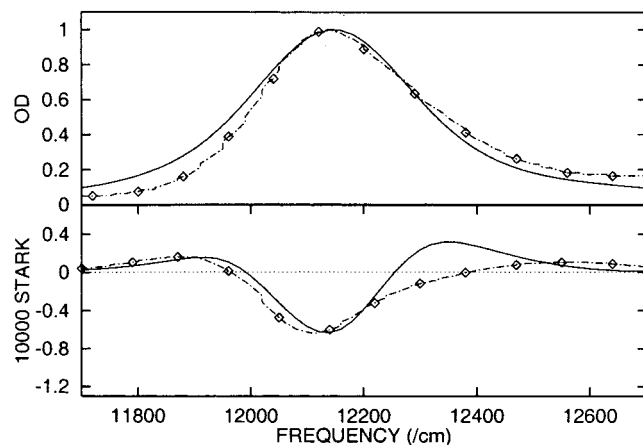


Figure 5. Best fit to 77 K absorption and Stark ($=\Delta OD$ at $E_s = 10^5$ V/cm) spectra (diamonds) for the B820 dimer subunit from *Rsp. rubrum*. The spectra are calculated with a parallel dimer model and $\sigma = \Gamma = 120$ cm^{-1} , $\kappa = 1.2$, and $\Delta\mu = 1.25$ D. Other parameters as in Figure 3. Experimental spectra reproduced from Beekman et al.⁷

(reassociated LH1) complex. As before, we initially use the Bchl *a* parameters given in section 4. The aggregate is modeled as a ring of 32 pigments, in accordance with the low-resolution structure.¹¹ Since no detailed atomic-resolution structure is available for LH1, we assume the transition dipole moments to be in-plane and tangent to the ring. The former is consistent with linear dichroism measurements and with the structure of the related LH2 complex. To mimic the LH2

structure more closely, a second structure is considered, where the orientation of every second pigment is reversed. These structures will be denoted as a ring of parallel and antiparallel dimers, respectively. The intermolecular interactions are calculated with dipole–dipole coupling, and scaled such that the interaction between neighboring pigments is 230 cm^{-1} , the same value used above for the B820 dimer subunit, and similar to the nearest-neighbor interaction in LH2.²⁷

In Figure 6 the experimental spectrum is compared with simulated spectra where the inhomogeneity ratio σ/Γ varied between 0 and 4, and the structural disorder θ_0 between 0° and 40° . The simulated spectra are remarkably similar to those obtained for dimers in Figure 3, i.e., a type I (second-derivative) shaped spectrum for the ring of parallel dimers and a much smaller type II (first-derivative) shaped spectrum for the ring of antiparallel dimers. The similarity of the dimer and ring spectra is in agreement with the expressions obtained in section 3. The energetic and structural disorder cause large shifts in the spectra, most likely due to the fact that several forbidden transitions lay within the width of the absorption band, and these become partially allowed by the disorder. However, the effect of disorder on the shape of the Stark spectrum is even less than in the dimer case, and hardly affects the fit with experiment.

Although the parameters used for the simulated spectra in Figure 6 were taken from separate experiments and should thus at least be of the correct order of magnitude, none of the spectra in this figure reproduces the experimental Stark spectrum: the simulated spectra of the ring of parallel dimers are three times weaker than experiment. Moreover, they have a second-derivative shape, instead of the observed first-derivative shape of the experimental spectrum. The simulated spectra of the ring of antiparallel dimers do have a first-derivative shape, but their magnitude is even weaker, and their sign is wrong.

To resolve the discrepancy, an explanation must be found for the large first-derivative components. Equations 15 and 16 suggest several possible origins for this component. First, in both expressions the second term has a first-derivative shape. Its contribution scales with $\kappa^2 - 2$, and may be enhanced for example by taking a stronger $S_1 \rightarrow S_2$ transition than assumed so far. The results of increasing κ up to 4 are shown in Figure 7. This is indeed sufficient to reproduce the magnitude of the experimental spectrum. It makes little difference which of the two structural models is used. The experimental spectrum is shifted with respect to the simulated one, and thus the fit may be further improved by adding a stronger second-derivative component to the spectrum. This may be caused by a difference dipole moment induced by matrix fields in the protein.^{5,7}

Unfortunately, the present fit suffers from several difficulties because of the large increase of κ that is needed. First, it implies that the total excited state oscillator strength is 16 times stronger than the ground state absorption, which has not been observed.²⁴ Second, Figures 7C and D indicate that these values for κ induce similar strong first-derivative spectra in the dimer, in contradiction with experiment. Since it is highly unlikely that a large change of the excited state absorption of the single pigments should occur upon the formation of the LH1 aggregate from its B820 subunits, this model is unrealistic.

Another option is to enhance the type II contribution in equation¹⁶ which also has a first derivative shape, by increasing $\Delta\mu$. This contribution is present in the simulated spectra of the ring of anti-parallel dimers (Figure 6C), but with a very small amplitude. The simplest way to enhance it, is by

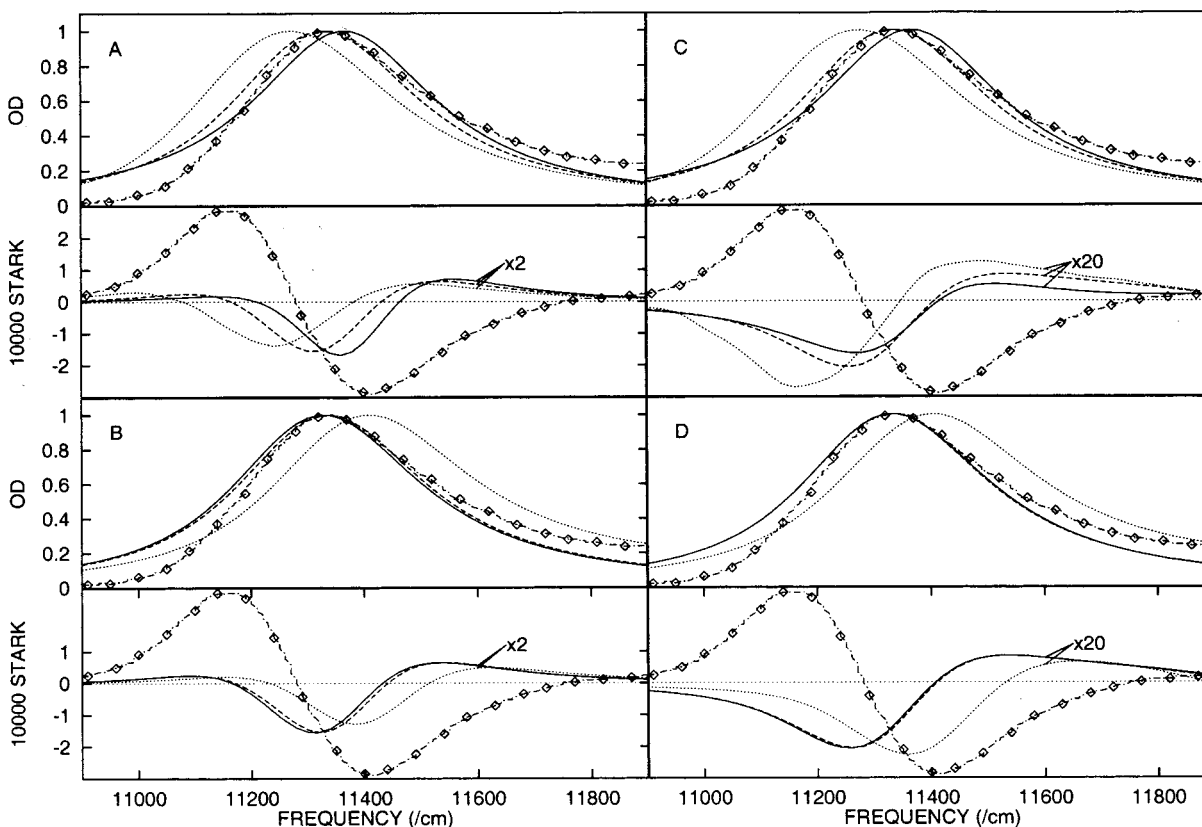


Figure 6. Simulated absorption and Stark ($=\Delta OD$ at $E_s = 10^5$ V/cm) spectra for a circular Bchl *a* aggregate ($N = 32$), and experimental 77 K spectra (diamonds) for B873 (reassociated LH1) from *Rsp. rubrum*. (A and B) Ring of parallel dimers (see text) with (A) energetic disorder: $\sigma/\Gamma = 0$ (solid), 1 (dashed), and 4 (dotted). (B) Structural disorder: $\theta_0 = 0^\circ$ (solid), 10° (dashed), and 40° (dotted), for $\sigma = \Gamma = 155$ cm^{-1} . (C and D) Same simulations for a ring of antiparallel dimers (see text). Other parameters: $\Omega = 11890$ cm^{-1} , $\mu = 6.2$ D; $\kappa = 1$, $\Delta\mu = 1.45$ D. J_{nm} from dipole-dipole interaction (see text). $\epsilon = 2.0$. As indicated, the simulated spectra are multiplied by 2 (A and B) or 20 (C and D). Experimental spectra reproduced from Beekman *et al.*⁷

increasing the difference dipole moment ($\Delta\mu$) or the local field correction factor. However, the required changes are again large and raise similar objections as for the κ -case discussed above.

This type II contribution can also be enhanced with parameters that do not affect the monomer spectra, e.g., by reducing the bandwidth of the one-exciton manifold. This was discussed for the dimer case below equation 14. It is shown in Figure 8A, where the intermolecular interactions are reduced by up to a factor 4. Indeed, with decreasing interaction, the exciton bandwidth decreases, and the magnitude of the simulated Stark spectrum is enhanced. However, the increase is not sufficient because its magnitude cannot exceed that of the (type I) spectrum in the ring with parallel dimers (Figure 6A). Moreover, as the magnitude approaches that of the type I contribution its shape changes to a second derivative. This is a typical behavior for type II contributions since they interpolate between the different shapes. Thus, the type II contribution also cannot reproduce the experimental spectrum.

We have further varied the parameters that define the aggregate's geometry. There is, however, no indication that any of these will reproduce the required large first derivative Stark spectrum. In addition to Figure 8A, discussed above, this is further confirmed by Figure 8B, where the energy difference between the optical gaps of the two pigments in the dimer subunit was varied. This leads to a minor enhancement of the type II contribution in the ring of antiparallel dimers. Also, the out-of-plane angle of the dipole moments (up to 30°) has no notable effects on the Stark spectrum (not shown). Other geometrical parameters were not varied.

In Figure 9, the parameter optimizations discussed above were combined to yield our best fit to experiment. Only σ/Γ , κ , and $\Delta\mu$ were varied, since the other parameters only have a minor effect. The fit to the experimental Stark spectrum is remarkably good. Deviations in the wings of the both the Stark and absorption spectra may be attributed to the relatively simple model used for spectral broadening.

In conclusion, a satisfactory fit of the experimental absorption and Stark spectrum of LH1 could be obtained with a model of excitonically interacting molecules, but the required parameters differ strongly from those obtained for its B820 dimer subunit and monomeric Bchl *a*. This indicates that the present model is incomplete and that additional states have to be considered, which play a role in the intact LH1, but not in its smaller subunits. This was proposed earlier on the basis of semi-empirical fit using the PEE2,⁵⁻⁸ but is now backed by simulated Stark spectra and a microscopic model of the molecular aggregate.

B. The LH2 Complex. Finally, we apply our analysis to the light-harvesting 2 (LH2) complex of *Rps. acidophila*. No dimer subunit has been isolated for this protein, but more detailed structural information is available. We use parameters which successfully reproduced experimental superradiance²⁰ and long time pump-probe spectra.²⁸ Thus LH2 is modeled by a ring of 18 pigments with orientations as in the crystal structure,⁹ and intermolecular interaction strengths from point charge calculations.²⁷ The chromophore parameters are initially taken as given in the beginning of this section, except that $\kappa = 0.9$, from the fits of Meier *et al.*^{28,20}

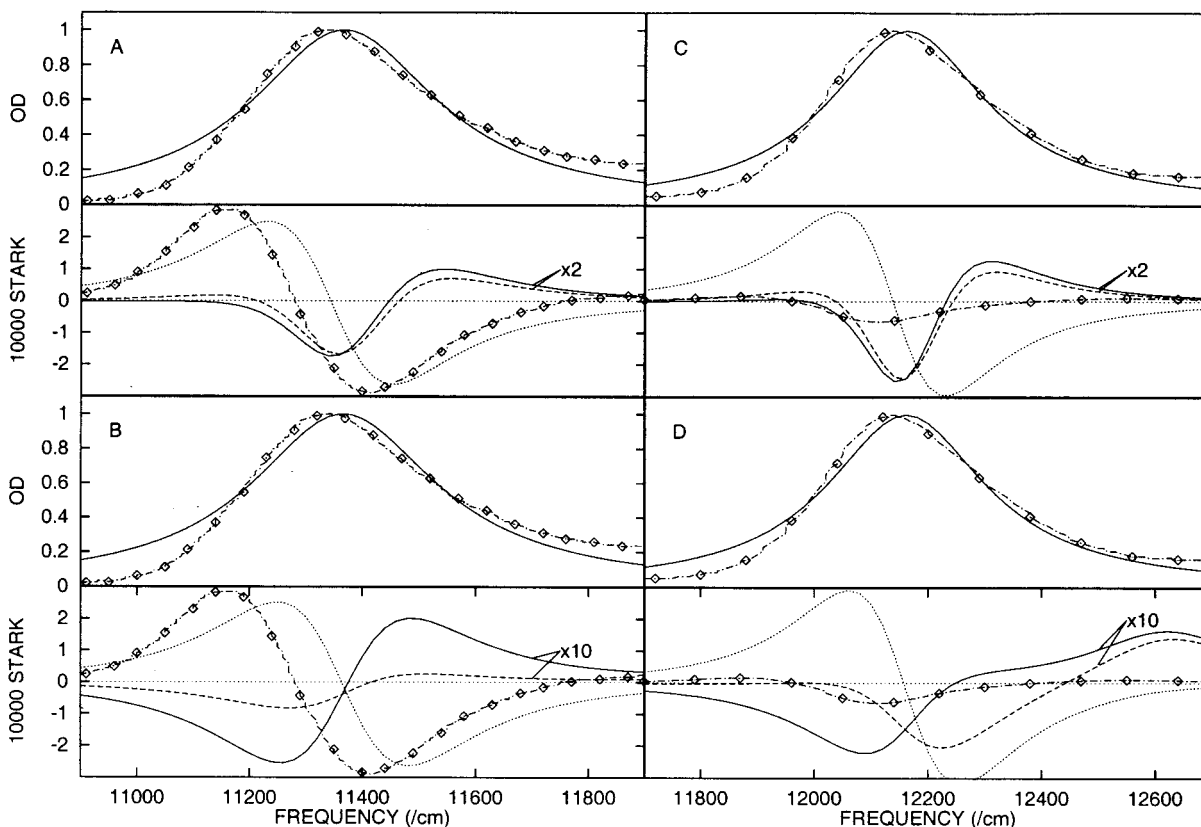


Figure 7. Simulated absorption and Stark ($=\Delta OD$ at $E_s = 10^5$ V/cm) spectra for ring of parallel (A) and antiparallel (B) Bchl *a* dimers, both in conjugation with experimental 77 K spectra (diamonds) for B873 (reassociated LH1) from *Rsp. rubrum*, and parallel (C) and antiparallel dimeric Bchl *a* aggregates, both in conjugation with experimental 77 K spectra (diamonds) for the B820 dimer subunit from *Rsp. rubrum*. (see text). In all panels $\kappa = 0$ (solid), 1 (dashed), and 4 (dotted). For the circular aggregates: $\sigma = 0$, $\Gamma = 200$ cm^{-1} . Other parameters as in figures 4 and 6. As indicated, the simulated spectra for $\kappa = 0$ and 1 are multiplied by 2 (A and C) or 10 (B and D). Experimental spectra reproduced from Beekman et al.⁷

Notwithstanding the more detailed structural information, the results are similar to those presented above for LH1, and we review them only briefly. Figure 10A shows simulated spectra for several inhomogeneity ratios σ/Γ between 0 and 4, together with the experimental spectra for LH2. The first-derivative shape of the Stark spectrum agrees with the roughly anti-parallel pigments in the dimer subunit of LH2, but its magnitude and sign do not match experiment. Energetic disorder leads to an overall red shift of both the absorption and Stark spectrum, but has very little effect on the shape of the spectra.

The fit to experiment can again be improved by increasing κ , μ , $\Delta\mu$ of ϵ . The former is illustrated in Figure 10B, where again a change to $\kappa > 4$ is required to reproduce the magnitude of the experimental Stark spectrum, a value that is too different from that in the monomeric Bchl *a*, to be caused by changes in the environment. Moreover, the fit of the LH2 spectrum in figure 10B, is not as good as that for LH1 in Figure 7, because the experimental LH2 spectrum is asymmetric and shows a shoulder on the red wing. Neither of these features is reproduced by the simulated spectra. Therefore, our results do not substantiate suggestions⁵ that the shoulder may be due to the red most exciton component of the LH2 ring.

Our analysis of the LH2 Stark spectrum confirms the conclusion drawn for LH1, i.e., that the spectrum can be fitted with an excitonic interaction model, but that the parameters differ considerably from those of the monomeric Bchl *a*.

6. Discussion

In this paper, four expressions for the Stark signal of molecular aggregates were presented and compared. These are

(i) The Green function expression (GFE, eq 6), derived from the third-order nonlinear response of the aggregate to the total (static + optical) electric field. Intermolecular interactions are treated within the local field approximation. With a modified rotating wave approximation (described above eq 6), only terms of lowest order in the ratio Γ/Ω of the dephasing and the optical gap were retained; (ii) The sum-over-states expression (SOS, eq C2), which provides an alternative description of the third order response function to the total electric field, and thus of the Stark signal; (iii) Liptay's perturbed eigenstate expression (PEE, eq A4).¹ This is obtained by calculating the transition dipole moments and transition frequencies of a multilevel molecule, up to second order in the static field; (iv) The commonly used simplified version of the perturbed eigenstate expression (PEE2, eq A6). This is obtained by retaining from the PEE, only the terms to lowest order in the ratio $\Gamma/\omega_{\beta\alpha}$ of the dephasing and the frequency separation between one-exciton levels.

Several similarities and differences between these four approaches have been observed in this paper. The PEE is elegant because it expresses the Stark spectrum as a sum of the contributions of individual transitions, which are shaped as the zeroth, first, and second derivative of the line shape function. In the PEE2, only the latter two are present, and their amplitudes are determined respectively by the difference in static polarizability ($\Delta\alpha$) between the excited state and the ground state and the difference in permanent dipole moment ($\Delta\mu$) between these two states. In the more general PEE, also the transition polarizability (α) and hyperpolarizability (β) need to be taken into consideration (see eq A5). In the ideal case when one

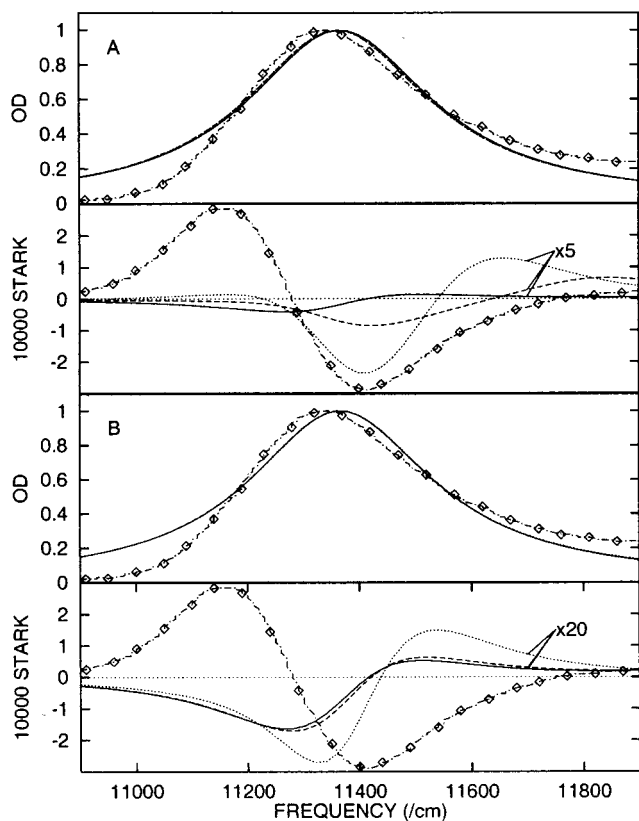


Figure 8. Simulated absorption and Stark ($=\Delta OD$ at $E_s = 10^5$ V/cm) spectra for ring antiparallel Bchl *a* dimers, and experimental 77 K spectra (diamonds) for B873 (reassociated LH1) from *Rsp. rubrum*. In A, all intermolecular interaction strengths are reduced by a factor 1 (solid), 2 (dashed), and 4 (dotted), with respect to Figure 6. In B, the energy difference between the two pigments in the dimeric subunits is varied from 0 to 100 cm^{-1} and 400 cm^{-1} while intermolecular interaction strengths are scaled such the excitonic bandwidth does not change. Other parameters as in Figure 7. As indicated, the simulated spectra are multiplied by 5 (A) or 20 (B). Experimental spectra reproduced from Beekman et al.⁷

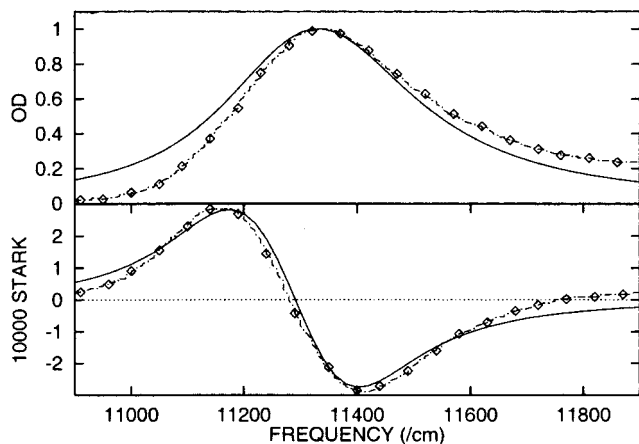


Figure 9. Best fit to 77 K absorption and Stark ($=\Delta OD$ at $E_s = 10^5$ V/cm) spectra (diamonds) for B873 (reassociated LH1) from *Rsp. rubrum*. The spectra are calculated for a ring of parallel dimers with $\sigma = \Gamma = 155$ cm^{-1} , $\kappa = 4$, and $\Delta\mu = 2.0$ D. Other parameters as in Figure 6. Experimental spectra reproduced from Beekman et al.⁷

transition dominates the absorption spectrum, the parameters can be determined by fitting the Stark spectrum with derivatives of the absorption spectrum. This has indeed been done for photosynthetic proteins.⁴⁻⁸ However, these approaches become problematic when quantitative calculations are attempted for

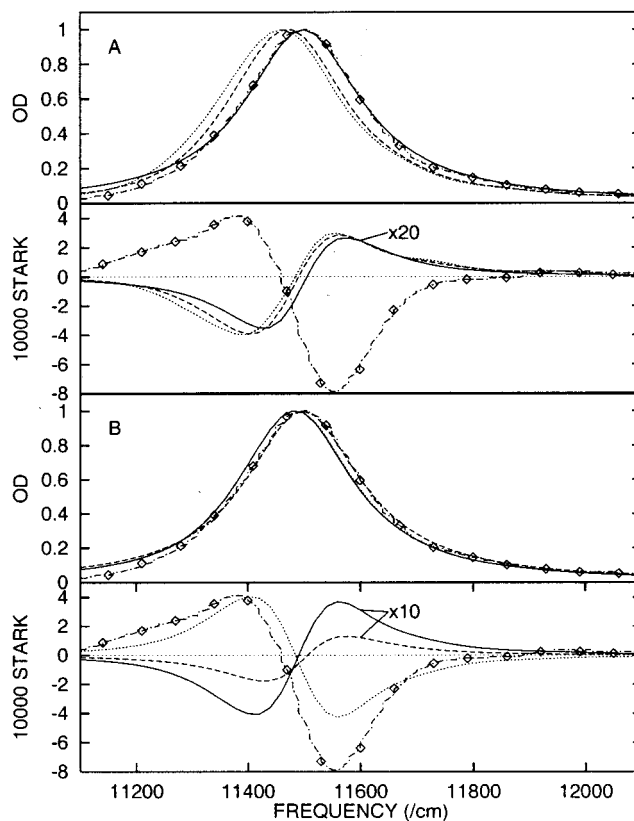


Figure 10. Simulated absorption and Stark ($=\Delta OD$ at $E_s = 10^5$ V/cm) spectra for a circular Bchl *a* aggregate ($N = 18$) and experimental 77 K spectra (diamonds) for LH2 from *Rps. acidophila*. Structure and intermolecular interaction: see text. (A) Energetic disorder: $\sigma/\Gamma = 0$ (solid), 2.2 (dashed), and 4 (dotted). (B) $\kappa = 0$ (solid), 0.9 (dashed), and 4 (dotted), for $\sigma = 0$ cm^{-1} and $\Gamma = 125$ cm^{-1} . Other parameters: $\Omega = 12100$ cm^{-1} , $\mu = 6.2$ D, $\kappa = 0.9$ (A), and $\Delta\mu = 1.45$ D. J_{nm} from Sauer et al (see text). $\epsilon = 2.0$. As indicated, the simulated spectra are multiplied by 20 (A) or 10 (B, except $\kappa = 4$). Experimental spectra reproduced from Beekman et al.⁸

such molecular aggregates. In that case, the PEE2 cannot be used because the condition $\omega_{\beta\alpha} \gg \Gamma$ does not in general hold, and the PEE contains singular terms which require careful cancellation.

At first sight, the GFE appears to be more complicated than the PEE approaches, for two reasons. First, the GFE contains products of line shape functions. When these are from the same transition (type I), the result corresponds to terms in the PEE2, but many terms contain products of different line shape functions (type II) which complicate the expression. Second, the GFE expresses the Stark signal in terms of the dipole moments ($\vec{\mu}_n$, $\Delta\vec{\mu}_n$, κ_n) of the individual pigments. While this is not in fundamental disagreement with the PEE, the elegant intermediate expression in terms of dipole moments and (hyper)-polarizabilities of one-exciton states is no longer possible with the GFE.

However, the superiority of the GFE becomes clear when the type II contributions are studied in more detail. On the one hand, they can be expressed as sums of type I contributions. Indeed, by carefully carrying out this procedure, we demonstrated that the GFE and PEE coincide, at least within the modified RWA for which the former was given. On the other hand, the type II contributions themselves avoid the singularities of the PEE, by interpolating between the zeroth-, first-, and second-derivative type I shapes. This is most obvious for the phenomenon that occurs when transitions are allowed between

one-exciton states, as is indeed the case for an antiparallel dimer (eq 14), or a circular aggregate (eqs 15 and 16). When the transition frequency is larger than the line width, it contributes mainly to the $\Delta\alpha$'s of the two states. But when the frequency becomes zero, it contributes to the $\Delta\mu$ of the resulting degenerate transition. This phenomenon is not represented in the PEE; when the transition frequency approaches zero, $\Delta\alpha$ becomes singular (eq A5), and must be carefully canceled out with other singular contributions from transition (hyper)polarizabilities (eq A5). In the GFE, however, this phenomenon is included in only one type II term which is directly related to that particular transition, and naturally changes from a first- to a second-derivative shape as the transition frequency approaches zero. This makes the GFE more convenient, both for numerical calculations, and because the GFE is more directly related to the dynamics of the aggregate, for interpretation. We illustrated this for symmetric aggregates. In the absence of such allowed transitions within the one-exciton band, the PEE2 could be more useful, but this is not generally the case for photosynthetic pigment-protein complexes. In addition, the PEE requires summation over all one- and two-exciton states, while, within the local field approximation, a summation over one-exciton states is sufficient for the GFE.

The SOS is in essence a less advanced version of the GFE. It expresses the Stark spectrum in terms of (transition) dipole moments for the one- and two-exciton states. We demonstrated that the expressions coincide within the modified RWA for which the GFE was given. But in more general cases, the SOS suffers from large canceling contributions (see ref 15 or eq C1) and requires summation over one- and two-exciton states, as well as a complicated model for ground state relaxation to avoid divergence.

In summary, we propose that the GFE is the most suitable expression for the Stark signal of molecular aggregates, and use the GFE for the numerical calculations in this paper.

An important result which follows from the GFE (eq 6), is that the formation of a molecular aggregate does not in general lead to an enhancement of the Stark signal. This is because type I contributions are converted to type II contributions with the same prefactors, while the amplitudes of the latter are smaller. In particular, if all line shape functions contributing to eq 6 are identical, the summations can be carried out analytically and the result is equal to the Stark signal of the uncoupled monomers. This situation occurs when the exciton bandwidth is small, or when the most strongly coupled pigments are parallel, so that prefactors of the type II contributions vanish. In other cases the amplitude of the Stark spectrum is typically reduced. This is confirmed by the numerical and analytical spectra presented throughout this paper.

Enhancement of the Stark signal is still possible if the intermolecular interaction causes narrowing of the line width functions, as occurs, e.g., in J-aggregates. But this is not generally the case in photosynthetic pigment protein aggregates. For this reason alone, the large first-derivative-shaped Stark spectra observed for LH1 and LH2 are remarkable and indicate that additional mechanisms play a role in these proteins. The experimental B820 spectrum is similar both in shape and magnitude to that of monomeric Bchl *a* and should be easier to model.

Stark and absorption spectra were simulated for LH1 and its B820 dimer subunit and of LH2 and compared to experimental

spectra. Initially, we used only parameters derived from ground and excited state absorption spectra and Stark spectra of the monomeric Bchl *a* molecule. From this starting point, we varied parameters one-by-one to improve the fit. The B820 spectrum is similar to that of monomeric Bchl *a* and was best represented by a dimer of parallel pigments, in agreement with the aforementioned general properties of the GFE. This differs from the crystal structure of LH2, where neighboring pigments were found to be antiparallel. The fit to the experimental Stark spectrum was, however, not quite satisfactory. In earlier studies, a better fit was obtained by a linear combination of the zeroth and second derivative of the absorption spectrum.⁷ However, our results show that a large zeroth-derivative contribution, i.e., a loss of dipole strength, does not result from intermolecular interaction alone, indicating that an alternative mechanism may be present.

With the initial parameter set, our simulated spectra for circular aggregates deviated strongly from the experimental Stark spectra of LH1 and LH2. A satisfactory fit could be obtained by increasing either the relative oscillator strength (κ^2) of the excited state absorption, or the difference dipole moment of the Bchl *a* molecule, with respect to the monomer, or by increasing the local field correction factor from its value used for the dimer. However, the required changes are large, and agree neither with the parameters observed in the monomeric Bchl *a* molecule, nor with the observed Stark spectrum of the B820 dimer subunit. A numerical survey was carried out by varying individual parameters and demonstrated that no set of parameters can simultaneously reproduce the magnitude of the observed Stark spectrum of LH1 and its B820 dimer subunit. We thus conclude that it is not possible to model the LH1 Stark spectrum with an excitonically coupled aggregate and that an alternative explanation must be found for the observed large spectrum. This has been previously suggested,^{5,7,8} and is now confirmed on the basis of quantitative calculations of the Stark spectra of molecular aggregates.

The most likely explanation for the observed large Stark spectrum is the presence of an additional state that does not occur in the monomeric pigments or the B820 dimer. To reproduce the required first derivative shape by a type II contribution, this state should be located at an energy above the one-exciton band. In addition, this type II term contributes a positive peak to the Stark spectrum at the position of the added state, even if the state itself carries no oscillator strength. Since such a feature has not been observed, its magnitude must be small, implying that the added state is located at an energy that is at least several thousand cm^{-1} above the one-exciton band. This in turn implies that the transition dipole moment between the one-exciton transitions and the added state must be of the order of 10 Debye or larger, to reproduce the magnitude of the observed spectrum. This is a reasonable value if the added state has a charge transfer character, since a charge separation of one electron between two neighboring Bchl *a* molecules in LH2, i.e., at ≈ 0.9 nm distance results in a permanent dipole moment of ≈ 50 D. It does, however, confirm that a state with charge transfer character is required, since any other state cannot produce sufficiently strong transitions.

Recently, detailed quantum mechanical calculations, including charge transfer states, have been carried out for LH2 of *Rps. acidophila*.²⁹ Although some attempts have been made to describe the effects of charge transfer states on the Stark

spectrum of the photosynthetic reaction center,³⁰ no general model for such spectra is as yet available for aggregates with charge transfer states. The development of such a model will be extremely useful.

Acknowledgment. The stay of OJGS at the University of Rochester was financed by a “TALENT” grant from the Netherlands Foundation for Scientific Research (NWO). The support of the Air Force Office of Scientific Research and the National Science Foundation is gratefully acknowledged. The authors thank S. Boxer and L.M.P. Beekman for allowing the use of their experimental spectra.

Appendix A: Perturbed Eigenstate Expression (PEE) for Stark Spectra

The conventional expression for the Stark signal of a multilevel molecule¹ is obtained by calculating how the static electric field affects its absorption spectrum. The molecule is defined by states a , with energy $\tilde{\epsilon}_a$ and dephasing rate γ_a , and by transition dipole moments $\tilde{\mu}_{ba}$ between states b and a . The linear absorption $\tilde{S}_a(\omega)$ with respect to the optical part (E_0) of the field in eq 4 is given by¹⁵

$$\tilde{S}_a(\omega) = \left(-\frac{1}{\hbar}\right) \text{Im} \left[\sum_{ba} P(a) \tilde{\mu}_{ab} \tilde{\mu}_{ba} \tilde{I}_{ba}(\omega) \right] E_0^* E_0 \quad (\text{A1})$$

with $P(a)$ the equilibrium population of state a , and $\tilde{I}_{ba}(\omega) = 1/(\omega - \tilde{\omega}_{ba} + i\Gamma_{ba})$ a complex line shape function, with $\hbar\tilde{\omega}_{ba} = \tilde{\epsilon}_b - \tilde{\epsilon}_a$ and $\Gamma_{ba} = (\gamma_b + \gamma_a)/2$. The “ \sim ” indicates quantities that are affected by the static field E_s . $P(a)$ and γ_a are assumed to be independent of E_s . The perturbation of $\tilde{\mu}_{ba}$ and $\tilde{\omega}_{ba}$ is formally expressed as

$$\begin{aligned} \tilde{\mu}_{ba} &= \mu_{ba} + \alpha_{ba} E_s + \beta_{ba} E_s E_s + \dots \\ \hbar\tilde{\omega}_{ba} &= \hbar\omega_{ba} - \Delta\mu_{ba} E_s - \frac{1}{2}\Delta\alpha_{ba} E_s E_s + \dots \end{aligned} \quad (\text{A2})$$

where the as yet undetermined tensors α_{ba} and β_{ba} are the transition polarizability and hyperpolarizability, $\Delta\alpha_{ba} \equiv \alpha_{bb} - \alpha_{aa}$ is the more familiar static difference polarizability, and $\Delta\mu_{ba} \equiv \mu_{bb} - \mu_{aa}$ the difference dipole moment between states b and a .

The Stark signal is defined by the change of the absorption $\tilde{S}_a(\omega)$ caused by the field E_s . The first-order perturbation:

$$S_E^{(1)}(\omega) = \left(-\frac{1}{\hbar}\right) \text{Im} \left[\sum_{ab} P(a) \left[(\mu_{ab}\alpha_{ba} + \alpha_{ab}\mu_{ba}) I_{ba}(\omega) - \frac{\mu_{ab}\Delta\mu_{ba}\mu_{ba}}{\hbar} I_{ba}^2(\omega) \right] \right] E_0^* E_s E_0 \quad (\text{A3})$$

carries information on α_{ba} and $\Delta\mu_{ba}$, but vanishes for isotropic samples. In the present paper, we therefore focus on the second-

order perturbation:

$$S_E(\omega) = \left(-\frac{1}{\hbar}\right) \text{Im} \left[\sum_{ab} P(a) \left[(\mu_{ab}\beta_{ba} + \alpha_{ab}\alpha_{ba} + \beta_{ab}\mu_{ba}) I_{ba}(\omega) - \frac{\mu_{ab}\Delta\mu_{ba}\alpha_{ba} + \alpha_{ab}\Delta\mu_{ba}\mu_{ba} + \mu_{ab}\Delta\alpha_{ba}\mu_{ba}/2}{\hbar} I_{ba}^2(\omega) + \frac{\mu_{ab}\Delta\mu_{ba}^2\mu_{ba}}{\hbar^2} I_{ba}^3(\omega) \right] \right] E_0^* E_s E_s E_0 \quad (\text{A4})$$

This result will be denoted the perturbed eigenstate expression (PEE) for $S_E(\omega)$. It is a product of a fourth-rank tensor and four fields. The signal $\langle S_E(\omega) \rangle$ for isotropic samples can be obtained by averaging over orientations, as described in Appendix B.

Several additional results facilitate the application of the PEE. First, the transition polarizability and hyperpolarizability can be calculated with time-independent perturbation theory. In the absence of dephasing, they are given by

$$\begin{aligned} \alpha_{ab} &= \sum_{c \neq b} \frac{\mu_{ac}\mu_{cb}}{\hbar\omega_{cb}} + \sum_{c \neq a} \frac{\mu_{cb}\mu_{ac}}{\hbar\omega_{ca}} \\ \beta_{ab} &= \sum_{c \neq ad \neq a} \frac{\mu_{cb}\mu_{ad}(\mu_{dc} - \delta_{dc}\mu_{aa})}{\hbar^2\omega_{ca}\omega_{da}} + \sum_{c \neq bd \neq b} \frac{\mu_{ac}(\mu_{cd} - \delta_{cd}\mu_{bb})\mu_{db}}{\hbar^2\omega_{cb}\omega_{db}} + \sum_{c \neq ad \neq b} \frac{\mu_{ca}\mu_{ad}\mu_{db}}{\hbar^2\omega_{ca}\omega_{db}} - \frac{1}{2}\mu_{ab} \left(\sum_{c \neq a} \frac{\mu_{ac}\mu_{ca}}{\hbar^2\omega_{ca}^2} + \sum_{c \neq b} \frac{\mu_{bc}\mu_{cb}}{\hbar^2\omega_{cb}^2} \right) \end{aligned} \quad (\text{A5})$$

Second, the line shape functions satisfy $d^n I_{ba}(\omega)/d\omega^n = (-1)^n n! I_{ba}^{n+1}(\omega)$. The imaginary part of the right-hand side coincides with the frequency dependent components of $S_E(\omega)$ in eq A4 which is thus a linear combination of the zeroth, first, and second derivative of the absorption line shape functions.

Third, when the transitions are sufficiently well separated to be distinguished in the absorption spectrum, $S_E(\omega)$ is a linear combination of the derivatives of $S_A(\omega)$. This result can be used to analyze experimental Stark spectra.

Finally, under the same condition, i.e., when the frequency separation ω_{bc} to the nearest other transition is larger than Γ_{ba} , leading contributions $S_E(\omega)$ can be distinguished by the power at which they scale with Γ_{ba} and ω_{bc} . The third term of eq A4 scales with $1/\Gamma_{ba}^3$ and is much larger than the second term which scales as $1/(\Gamma_{ba}^2\omega_{bc})$, unless the permanent dipole moments are absent or much smaller than the transition dipole moments. In that case the $\Delta\alpha_{ba}$ -dependent part of the second term is important. This leads to a simplified expression,

$$S_E(\omega) \approx \left(-\frac{1}{\hbar}\right) \text{Im} \left[-\frac{\mu_{ab}\Delta\alpha_{ba}\mu_{ba}/2}{\hbar} I_{ba}^2(\omega) + \frac{\mu_{ab}\Delta\mu_{ba}^2\mu_{ba}}{\hbar^2} I_{ba}^3(\omega) \right] E_0^* E_s E_s E_0 \quad (\text{A6})$$

which will be denoted PEE2. The first term scales with $1/(\Gamma_{ba}\omega_{bc}^2)$ and is thus smaller than the other terms, under the given conditions. No such simplification is found for $S_E^{(1)}$.

The expression of $S_E(\omega)$ as a linear combination of the zeroth, first, and second derivative of $S_A(\omega)$, is often used for the analysis of experimental Stark spectra, while the PEE2 is applied to interpret the coefficients of the components.^{4–8} Note, however, that the condition $\omega_{bc} \gg \Gamma_{ba}$ is not in general satisfied in a molecular aggregate. See main text for further discussion.

Appendix B: Stark Spectra of Isotropic Samples

The expressions for the Stark spectrum in eq 6, A4, and C2 are all given for a particular orientation of the molecule and expressed in the form

$$S_E(\omega) = A(\omega)E_0^*E_sE_sE_0 = \sum_{ijkl} A_{ijkl}(\omega)(E_0^*)_i(E_s)_j(E_s)_k(E_0)_l \quad (\text{B1})$$

i.e., as a product of a fourth-rank tensor and four electric fields. For isotropic samples, the Stark signal $\langle S_E(\omega) \rangle$ can be obtained by averaging over all molecular orientations. To carry out this procedure we first note that the fields are equal two by two. Moreover, E_s is real, and as the light is plane-polarized, E_0 is equal to a real vector multiplied by a phase factor. This phase factor can be ignored because of the multiplication with the complex conjugate. The Stark signal of the isotropic sample is then

$$\begin{aligned} \langle S_E(\omega) \rangle &= \langle \sum_{ijkl} A_{ijkl}(\omega)(E_0^*)_i(E_s)_j(E_s)_k(E_0)_l \rangle \\ &= \frac{1}{45} \sum_{ij} \left(5A_{ijji}(\omega) + [3\cos^2(\chi) - 1] \left[3 \frac{A_{ijij} + A_{ijji}}{2} - A_{ijji} \right] \right) |E_s|^2 |E_0|^2 \quad (\text{B2}) \end{aligned}$$

where χ is the angle between the optical and static fields. For simplicity, many experiments are carried out at magic angle ($\cos \chi = 1/\sqrt{3}$), and the signal depends only on nine of the 81 elements of the tensor. Angle-dependent measurements provide information on the other tensor components.

Appendix C: Calculation of Stark Spectra Using the Sum-Over-States expression of $\chi^{(3)}$

Equation 6 can alternatively be derived from eq 5 by evaluating $\chi^{(3)}(-\omega; 0, 0, \omega)$ with the sum-over-states (SOS) expression.¹⁵ The aggregate of three level molecules is described by the Hamiltonian of eq 2 and the dipole operator by eq 3. As illustrated in Figure 1, we distinguish the ground state g , one-exciton states denoted α, β, \dots , and two-exciton states denoted ν, \dots . By retaining only those terms that fall within the modified RWA introduced above eq 6 while considering that all transition dipole moments $\mu_{\beta\alpha}$ within the one-exciton band originate from permanent dipole moments of the monomeric molecules, the following expression is obtained for the Stark signal:

$$\begin{aligned} S_E(\omega) &= \left(-\frac{1}{\hbar} \right)^3 \text{Im} \left[\sum_{\gamma\beta\alpha} \mu_{g\gamma} \mu_{\gamma\beta} \mu_{\beta\alpha} \mu_{\alpha g} I_{\gamma g}(\omega) I_{\beta g}(\omega) I_{\alpha g}(\omega) + \right. \\ &\quad \sum_{\beta\alpha} \sum_{\nu} \mu_{g\beta} \mu_{\beta\nu} \mu_{\nu\alpha} \mu_{\alpha g} I_{\beta g}(\omega) I_{\nu g}(\omega) I_{\alpha g}(\omega) + \\ &\quad \sum_{\beta\alpha} \mu_{g\beta} \mu_{\beta g} \mu_{g\alpha} \mu_{\alpha g} I_{\beta g}(\omega) I_{g g}(\omega) I_{\alpha g}(\omega) + \\ &\quad \sum_{\beta\alpha} \mu_{g\alpha} \mu_{\beta g} \mu_{g\beta} \mu_{\alpha g} I_{\alpha g}(\omega) I_{\alpha\beta}(\omega) I_{\alpha g}(\omega) + \\ &\quad \sum_{\beta\alpha} \mu_{g\beta} \mu_{g\alpha} \mu_{\alpha g} \mu_{\beta g} I_{\beta g}(\omega) I_{g g}(0) I_{\alpha g}(0) + \\ &\quad \sum_{\beta\alpha} \mu_{g\beta} \mu_{\alpha g} \mu_{g\alpha} \mu_{\beta g} I_{\beta g}(\omega) I_{g g}(0) I_{g\alpha}(0) + \\ &\quad \left. \sum_{\gamma\alpha} \mu_{g\alpha} \mu_{g\gamma} \mu_{\alpha g} \mu_{\gamma g} I_{\alpha g}(\omega) I_{\alpha\gamma}(0) I_{\alpha g}(0) + \right. \\ &\quad \left. \sum_{\gamma\alpha} \mu_{g\alpha} \mu_{\alpha g} \mu_{g\gamma} \mu_{\gamma g} I_{\alpha g}(\omega) I_{\alpha\gamma}(0) I_{g\gamma}(0) \right] E_0^* E_s E_s E_0 \quad (\text{C1}) \end{aligned}$$

The first term of eq C1 coincides with the first term of equation 6 since $\mu_{\beta\alpha} = D_{\beta\alpha}^{(1)}$. The next three terms can be combined because within the rotating wave approximation; the frequency in all off-resonant line shape functions can be replaced by the optical gap Ω . Finally, the last four terms partially cancel in pairs, the result of which scales with $(\Gamma/\Omega)^2$ and can be ignored. Thus,

$$\begin{aligned} S_E(\omega) &= \left(-\frac{1}{\hbar} \right)^3 \text{Im} \left[\sum_{\gamma\beta\alpha} \mu_{g\gamma} \mu_{\gamma\beta} \mu_{\beta\alpha} \mu_{\alpha g} I_{\gamma g}(\omega) I_{\beta g}(\omega) I_{\alpha g}(\omega) - \right. \\ &\quad \sum_{\beta\alpha} \mu_{g\beta} \left(\sum_{\nu} \mu_{\beta\nu} \mu_{\nu\alpha} - \mu_{\beta g} \mu_{g\alpha} - \right. \\ &\quad \left. \left. \delta_{\beta\alpha} \sum_{\gamma} \mu_{\gamma g} \mu_{g\gamma} \right) \mu_{\alpha g} I_{\beta g}(\omega) I_{\alpha g}(\omega) \right] \frac{1}{\Omega} E_0^* E_s E_s E_0 = \\ &\quad \left(-\frac{1}{\hbar} \right)^3 \text{Im} \left[\sum_{\gamma\beta\alpha n m} \mu_{g\gamma} \phi_{\gamma}^*(n) \Delta \bar{\mu}_n \phi_{\beta}(n) \phi_{\beta}^*(m) \Delta \bar{\mu}_m \phi_{\alpha}(m) \mu_{\alpha g} \right. \\ &\quad \left. I_{\gamma g}(\omega) I_{\beta g}(\omega) I_{\alpha g}(\omega) - \right. \\ &\quad \left. \sum_{\beta\alpha n} \mu_{g\beta} \phi_{\beta}^*(n) (\kappa_n^2 - 2) \bar{\mu}_n^* \bar{\mu}_n \phi_{\alpha}(n) \mu_{\alpha g} I_{\beta g}(\omega) I_{\alpha g}(\omega) \right] \frac{1}{\Omega} E_0^* E_s E_s E_0 \quad (\text{C2}) \end{aligned}$$

which coincides with eq 6.

Appendix D: Comparison of the GFE and PEE for the Stark Signal

The GFE (eq 6) can be compared with the PEE (eq A4), by expanding all type II contributions as sums of type I contributions:

$$\begin{aligned} I_{\beta g}(\omega) I_{\alpha g}(\omega) &= -\frac{I_{\beta g}(\omega)}{\omega_{\alpha\beta}} - \frac{I_{\alpha g}(\omega)}{\omega_{\beta\alpha}} \\ I_{\beta g}^2(\omega) I_{\alpha g}(\omega) &= -\frac{I_{\beta g}^2(\omega)}{\omega_{\alpha\beta}} - \frac{I_{\beta g}(\omega)}{\omega_{\alpha\beta}^2} + \frac{I_{\alpha g}(\omega)}{\omega_{\beta\alpha}^2} \\ I_{\gamma g}(\omega) I_{\beta g}(\omega) I_{\alpha g}(\omega) &= \frac{I_{\gamma g}(\omega)}{\omega_{\alpha\gamma} \omega_{\beta\gamma}} + \frac{I_{\beta g}(\omega)}{\omega_{\alpha\beta} \omega_{\gamma\beta}} + \frac{I_{\alpha g}(\omega)}{\omega_{\beta\alpha} \omega_{\gamma\alpha}} \quad (\text{D1}) \end{aligned}$$

with $\omega_{\beta\alpha} \equiv \Omega_{\beta} - \Omega_{\alpha}$. To avoid singularities, we assume that

all one-exciton states have different energies and single out cases where one or more indices are equal.

$$\begin{aligned}
 S_E(\omega) &= \left(-\frac{1}{\hbar}\right)^3 \text{Im} \left[\sum_{\gamma\beta\alpha} \mu_{g\gamma} D_{\gamma\beta}^{(1)} D_{\beta\alpha}^{(1)} \mu_{\alpha g} I_{\gamma g}(\omega) I_{\beta g}(\omega) I_{\alpha g}(\omega) - \right. \\
 &\quad \left. \sum_{\beta\alpha} \mu_{g\beta} D_{\beta\alpha}^{(2)} \mu_{\alpha g} I_{\beta g}(\omega) I_{\alpha g}(\omega) \frac{1}{\Omega} \right] E_0^* E_s E_s E_0 \\
 &= \left(-\frac{1}{\hbar}\right)^3 \text{Im} \left[\sum_{\alpha} \mu_{g\alpha} D_{\alpha\alpha}^{(1)} D_{\alpha\alpha}^{(1)} \mu_{\alpha g} I_{\alpha g}^3(\omega) + \right. \\
 &\quad \sum_{\gamma\neq\alpha} \mu_{g\gamma} D_{\gamma\alpha}^{(1)} D_{\alpha\alpha}^{(1)} \mu_{\alpha g} \left(-\frac{I_{\alpha g}^2(\omega)}{\omega_{\gamma\alpha}} - \frac{I_{\alpha g}(\omega)}{\omega_{\gamma\alpha}^2} + \frac{I_{\gamma g}(\omega)}{\omega_{\alpha\gamma}^2} \right) + \\
 &\quad \sum_{\beta\neq\alpha} \mu_{g\alpha} D_{\alpha\beta}^{(1)} D_{\beta\alpha}^{(1)} \mu_{\alpha g} \left(-\frac{I_{\alpha g}^2(\omega)}{\omega_{\beta\alpha}} - \frac{I_{\alpha g}(\omega)}{\omega_{\beta\alpha}^2} + \frac{I_{\beta g}(\omega)}{\omega_{\alpha\beta}^2} \right) + \\
 &\quad \sum_{\beta\neq\alpha} \mu_{g\beta} D_{\beta\beta}^{(1)} D_{\beta\alpha}^{(1)} \mu_{\alpha g} \left(-\frac{I_{\beta g}^2(\omega)}{\omega_{\alpha\beta}} - \frac{I_{\beta g}(\omega)}{\omega_{\alpha\beta}^2} + \frac{I_{\alpha g}(\omega)}{\omega_{\beta\alpha}^2} \right) + \\
 &\quad \sum_{\beta\neq\alpha} \sum_{\gamma\neq\beta,\alpha} \mu_{g\gamma} D_{\gamma\beta}^{(1)} D_{\beta\alpha}^{(1)} \mu_{\alpha g} \left(\frac{I_{\gamma g}(\omega)}{\omega_{\alpha\gamma}\omega_{\beta\gamma}} + \frac{I_{\beta g}(\omega)}{\omega_{\alpha\beta}\omega_{\gamma\beta}} + \frac{I_{\alpha g}(\omega)}{\omega_{\beta\alpha}\omega_{\gamma\alpha}} \right) - \\
 &\quad \sum_{\alpha} \mu_{g\alpha} D_{\alpha\alpha}^{(2)} \mu_{\alpha g} I_{\alpha g}^2(\omega) \frac{1}{\Omega} - \\
 &\quad \left. \sum_{\beta\neq\alpha} \mu_{g\beta} D_{\beta\alpha}^{(2)} \mu_{\alpha g} \left(-\frac{I_{\beta g}(\omega)}{\omega_{\alpha\beta}} - \frac{I_{\alpha g}(\omega)}{\omega_{\beta\alpha}} \right) \frac{1}{\Omega} \right] E_0^* E_s E_s E_0 \quad (\text{D2})
 \end{aligned}$$

Next, by changing indices, and rearranging the order of the terms

$$\begin{aligned}
 S_E(\omega) &= \left(-\frac{1}{\hbar}\right)^3 \text{Im} \left[\sum_{\beta} \left(\sum_{\gamma,\delta\neq\beta} \frac{\mu_{g\beta} D_{\beta\delta}^{(1)} D_{\delta\gamma}^{(1)} \mu_{\gamma\beta}}{\omega_{\gamma\beta}\omega_{\delta\beta}} - \right. \right. \\
 &\quad \sum_{\gamma\neq\beta} \frac{\mu_{g\beta} D_{\beta\beta}^{(1)} D_{\beta\gamma}^{(1)} \mu_{\gamma\beta}}{\omega_{\gamma\beta}^2} + \sum_{\gamma\neq\beta} \frac{\mu_{g\beta} D_{\beta\gamma}^{(2)} \mu_{\gamma\beta}}{\omega_{\gamma\beta}\Omega} + \\
 &\quad \sum_{\gamma,\delta\neq\beta} \frac{\mu_{g\gamma} D_{\gamma\delta}^{(1)} D_{\delta\beta}^{(1)} \mu_{\beta\gamma}}{\omega_{\delta\beta}\omega_{\gamma\beta}} - \sum_{\gamma\neq\beta} \frac{\mu_{g\gamma} D_{\gamma\beta}^{(1)} D_{\beta\beta}^{(1)} \mu_{\beta\gamma}}{\omega_{\gamma\beta}^2} + \\
 &\quad \sum_{\gamma\neq\beta} \frac{\mu_{g\gamma} D_{\gamma\beta}^{(2)} \mu_{\beta\gamma}}{\omega_{\gamma\beta}\Omega} - \sum_{\gamma\neq\beta} \frac{\mu_{g\beta} D_{\beta\gamma}^{(1)} D_{\gamma\beta}^{(1)} \mu_{\beta\gamma}}{\omega_{\gamma\beta}^2} + \\
 &\quad \left. \sum_{\gamma,\delta\neq\beta} \frac{\mu_{g\gamma} D_{\gamma\beta}^{(1)} D_{\beta\delta}^{(1)} \mu_{\delta\gamma}}{\omega_{\delta\beta}\omega_{\gamma\beta}} \right) I_{\beta g}(\omega) - \\
 &\quad \sum_{\beta} \left(\sum_{\gamma\neq\beta} \frac{\mu_{g\beta} D_{\beta\beta}^{(1)} D_{\beta\gamma}^{(1)} \mu_{\gamma\beta}}{\omega_{\gamma\beta}} + \sum_{\gamma\neq\beta} \frac{\mu_{g\gamma} D_{\gamma\beta}^{(1)} D_{\beta\beta}^{(1)} \mu_{\beta\gamma}}{\omega_{\gamma\beta}} + \right. \\
 &\quad \left. \sum_{\gamma\neq\beta} \frac{\mu_{g\beta} D_{\beta\gamma}^{(1)} D_{\gamma\beta}^{(1)} \mu_{\beta\gamma}}{\omega_{\gamma\beta}} + \frac{\mu_{g\beta} D_{\beta\beta}^{(2)} \mu_{\beta\gamma}}{\Omega} \right) I_{\beta g}^2(\omega) + \\
 &\quad \left. \sum_{\beta} \mu_{g\beta} D_{\beta\beta}^{(1)} D_{\beta\beta}^{(1)} \mu_{\beta\beta} I_{\beta g}^3(\omega) \right] E_0^* E_s E_s E_0 \quad (\text{D3})
 \end{aligned}$$

This can be further recast in the form

$$\begin{aligned}
 S_E(\omega) &= \left(-\frac{1}{\hbar}\right)^3 \text{Im} \left[\sum_{\beta} \left[\left(\sum_{\gamma\neq\beta} \frac{\mu_{g\gamma} D_{\gamma\beta}^{(1)} \sum_{\delta\neq\beta} \frac{D_{\beta\delta}^{(1)} \mu_{\delta\gamma}}{\omega_{\delta\beta}} + \right. \right. \\
 &\quad \mu_{g\beta} \left(\sum_{\gamma,\delta\neq\beta} \frac{(D_{\beta\delta}^{(1)} - \delta_{\gamma\delta} D_{\beta\beta}^{(1)}) D_{\delta\gamma}^{(1)} \mu_{\gamma\beta}}{\omega_{\gamma\beta}\omega_{\delta\beta}} + \sum_{\gamma\neq\beta} \frac{D_{\beta\gamma}^{(2)} \mu_{\gamma\beta}}{\omega_{\gamma\beta}\Omega} - \right. \\
 &\quad \left. \left. \frac{1}{2} \sum_{\gamma\neq\beta} \frac{D_{\beta\gamma}^{(1)} D_{\gamma\beta}^{(1)}}{\omega_{\gamma\beta}^2} \mu_{\beta g} \right) + \left(\sum_{\gamma,\delta\neq\beta} \frac{\mu_{g\gamma} (D_{\gamma\delta}^{(1)} - \delta_{\gamma\delta} D_{\beta\beta}^{(1)}) D_{\delta\beta}^{(1)}}{\omega_{\delta\beta}\omega_{\gamma\beta}} + \right. \right. \\
 &\quad \left. \left. \sum_{\gamma\neq\beta} \frac{\mu_{g\gamma} D_{\gamma\beta}^{(2)}}{\omega_{\gamma\beta}\Omega} - \frac{1}{2} \mu_{g\beta} \sum_{\gamma\neq\beta} \frac{D_{\beta\gamma}^{(1)} D_{\gamma\beta}^{(1)}}{\omega_{\gamma\beta}^2} \right) \mu_{\beta g} \right] I_{\beta g}(\omega) - \\
 &\quad \left(\mu_{g\beta} D_{\beta\beta}^{(1)} \sum_{\gamma\neq\beta} \frac{D_{\beta\gamma}^{(1)} \mu_{\gamma\beta}}{\omega_{\gamma\beta}} + \sum_{\gamma\neq\beta} \frac{\mu_{g\gamma} D_{\gamma\beta}^{(1)}}{\omega_{\gamma\beta}} D_{\beta\beta}^{(1)} \mu_{\beta g} + \right. \\
 &\quad \left. \mu_{g\beta} \left(\sum_{\gamma\neq\beta} \frac{D_{\beta\gamma}^{(1)} D_{\gamma\beta}^{(1)}}{\omega_{\gamma\beta}} + \frac{D_{\beta\beta}^{(2)}}{\Omega} \right) \mu_{\beta g} \right) I_{\beta g}^2(\omega) + \\
 &\quad \left. \mu_{g\beta} D_{\beta\beta}^{(1)} D_{\beta\beta}^{(1)} \mu_{\beta\beta} I_{\beta g}^3(\omega) \right] E_0^* E_s E_s E_0 \quad (\text{D4})
 \end{aligned}$$

To compare this result to the PEE, we start with eq A4 and A5, apply this to an aggregate of three level molecules, and retain from the former only leading terms within the modified RWA as defined above eq 6. Those terms now coincide with eq D4.

References and Notes

- (1) Liptay, W. Dipole moments and polarizabilities of molecules in excited electronic states. In *Excited States*; Lim, E., Ed.; Academic Press: New York, 1974.
- (2) Lockhart, D. J.; Boxer, S. G. *Biochemistry* **1986**, *26*, 664–668.
- (3) Lockhart, D. J.; Boxer, S. G. *Proc. Natl. Acad. Sci. U.S.A.* **1988**, *85*, 107–111.
- (4) Middendorf, T. R.; Mazzola, L. T.; Lao, K. L.; Steffen, M. A.; Boxer, S. G. *Biochem. Biophys. Acta* **1993**, *1143*, 223–234.
- (5) Gottfried, D. S.; Stocker, J. W.; Boxer, S. G. *Biochem. Biophys. Acta* **1991**, *1059*, 63–75.
- (6) Boxer, S. G. Stark spectroscopy of photosynthetic systems. In *Biophysical Techniques in Photosynthesis*; Ames, A., Hoff, A. J., Eds.; Kluwer Academic Publishers: Boston, 1996.
- (7) Beekman, L. M. P.; Steffen, M. A.; van Stokkum, I. H. M.; Olsen, J. D.; Hunter, C. N.; Boxer, S. G.; van Grondelle, R. *J. Phys. Chem. B* **1997**, *101*, 7284–7292.
- (8) Beekman, L. M. P.; Frese, R. N.; Fowler, G. J. S.; Picorel, R.; Cogdell, R. J.; van Stokkum, I. H. M.; Hunter, C. N.; van Grondelle, R. *J. Phys. Chem. B* **1997**, *101*, 7293–7301.
- (9) McDermott, G.; Prince, S.; Freer, A.; Hawthornthwaite-Lawless, A.; Papiz, M.; Cogdell, R. J.; Isaacs, N. W. *Nature* **1995**, *374*, 517–524.
- (10) Koepke, J.; Hu, X.; Muenke, C.; Schulten, K.; Michel, H. *Structure* **1996**, *4*, 581–597.
- (11) Karrasch, S.; Bullough, P. A.; Ghosh, R. *EMBO J.* **1995**, *14*, 631–638.
- (12) Visschers, R. W.; Chang, M. C.; van Mourik, F.; Parkes-Loach, P. S.; Heller, B. A.; Loach, P. A.; van Grondelle, R. *Biochemistry* **1991**, *30*, 5734–5742.
- (13) Khidkele, V.; Chernyak, V.; Mukamel, S. *J. Chem. Phys.* **1996**, *105*, 8543–8555.
- (14) Kühn, O.; Chernyak, V.; Mukamel, S. *J. Chem. Phys.* **1996**, *105*, 8586–8601.
- (15) Mukamel, S. *Principles of Nonlinear Optical Spectroscopy*; Oxford University Press: New York, 1995.
- (16) Chernyak, V.; Mukamel, S. *Phys. Rev. B* **1993**, *48*, 2470–2478.
- (17) Chernyak, V.; Mukamel, S. *J. Opt. Soc. Am. B* **1996**, *13*, 1302–1307.
- (18) Chernyak, V.; Yokojima, S.; Meier, T.; Mukamel, S. *Phys. Rev. B* **1998**, *58*, 4496.
- (19) Chernyak, V.; Wang, N.; Mukamel, S. *Phys. Rep.* **1995**, *263*, 213–309.
- (20) Meier, T.; Zhao, Y.; Chernyak, V.; Mukamel, S. *J. Chem. Phys.* **1997**, *107*, 3876–3893.

- (21) Chernyak, V.; Mukamel, S. *J. Chem. Phys.* **1996**, *104*, 444–459.
- (22) Scherz, A.; Rosenbach-Belkin, V. The spectral properties of chlorophyll and bacteriochlorophyll dimers; A Comparative Study. In *The Photosynthetic Bacterial Reaction Center, Structure and Dynamics*; Breton, J., Vermeglio, A., Eds.; Plenum Press; New York, 1988.
- (23) Sauer, K.; Lindsay-Smith, J. R.; Schultz, A. J. *J. Am. Chem. Soc.* **1966**, *88*, 2681–2688.
- (24) Becker, M.; Nagarajan, V.; Parson, W. W. *J. Am. Chem. Soc.* **1991**, *113*, 6840–6848.
- (25) Renge, I. *Chem. Phys.* **1992**, *167*, 173–184.
- (26) Lao, K.; Moore, L. J.; Zhou, H.; Boxer, S. G. *J. Phys. Chem.* **1994**, *99*, 496–500.
- (27) Sauer, K.; Cogdell, R. J.; Prince, S. M.; Freer, A.; Isaacs, N. W.; Scheer, H. *Photochem. Photobiol.* **1996**, *64*, 564–576.
- (28) Meier, T.; Chernyak, V.; Mukamel, S. *J. Phys. Chem. B* **1997**, *101*, 7332–7342.
- (29) Alden, R. G.; Johnson, E.; Nagarajan, V.; Parson, W. W.; Law, C. J.; Cogdell, R. J. *J. Phys. Chem. B* **1997**, *101*, 4667–4680.
- (30) Scherer, P. O. J.; Fischer, S. F. *Chem. Phys. Lett* **1986**, *131*, 153–159.